Methionine oxidation of Carbohydrate-Active enZymes during white-rot wood decay

Lise Molinelli[1,2], Elodie Drula[1,3], Jean-Charles Gaillard[4], David Navarro[1], Jean Armengaud[4], Jean-Guy Berrin[1], Thierry Tron[2], Lionel Tarrago[1,#]

From:

[1] Aix Marseille Univ., INRAE, Biodiversité et Biotechnologies Fongiques, Marseille, France

[2] Aix Marseille Univ., CNRS, Centrale Marseille, ISM2, Marseille, France

[3] Architecture et Fonction des Macromolécules Biologiques (AFMB), CNRS, Aix-Marseille Université, Marseille, France

[4] Université Paris-Saclay, CEA, INRAE, Département Médicaments et Technologies pour la Santé (DMTS), SPI, 30200 Bagnols-sur-Cèze, France

[#] To whom correspondence should be address: Lionel Tarrago (lionel.tarrago@inrae.fr)

Running title (51 characters): MetO in CAZymes of white rot fungi during wood decay

Keywords: Carbohydrate-active enzymes, fungi, hydrogen peroxide, methionine oxidation, plant cell wall, redox proteomics, wood decay

Word count: 4428 (excluding Material and Methods)

Abstract

White-rot fungi employ secreted carbohydrate-active enzymes (CAZymes) along with reactive oxygen species (ROS), like hydrogen peroxide (H_2O_2), to degrade lignocellulose in wood. H_2O_2 serves as a co-substrate for key oxidoreductases during the initial decay phase. While the degradation of lignocellulose by CAZymes is well-documented, the impact of ROS on the oxidation of the secreted proteins remains unclear and the identity of the oxidized proteins is unknown. Methionine (Met) can be oxidized to Met sulfoxide (MetO) or Met sulfone ($MetO_2$) with potential deleterious, antioxidant, or regulatory effects. Other residues, like proline (Pro), can undergo carbonylation. Using the white-rot *Pycnoporus cinnabarinus* grown on aspen wood, we analyzed the Met content of the secreted proteins and their susceptibility to oxidation combining $H_2{}^{18}O_2$ with deep shotgun proteomics. Strikingly, their overall Met content was significantly lower (1.4%) compared to intracellular proteins (2.1%), a feature conserved in fungi but not in metazoans or plants. We evidenced that a catalase, widespread in white-rot fungi, protects the secreted proteins from oxidation. Our redox proteomics approach allowed identification of 49 oxidizable Met and 40 oxidizable Pro residues within few secreted proteins, mostly CAZymes. Interestingly, many of them had several oxidized residues localized in hotspots. Some Met, including those in GH7 cellobiohydrolases, were oxidized up to 47%, with a substantial percentage of sulfone (13%). These Met are conserved in fungal homologs, suggesting important functional roles. Our findings reveal that white-rot fungi safeguard their secreted proteins by minimizing their Met content and by scavenging ROS and pinpoint redox-active residues in CAZymes.

40 **Importance**

41 The study of lignocellulose degradation by fungi is critical for understanding the ecological and
42 industrial implications of wood decay. While carbohydrate-active enzymes (CAZymes) play a well-
43 established role in lignocellulose degradation, the impact of hydrogen peroxide (H_2O_2) on secreted
44 proteins remains unclear. This study aims at evaluating the effect of H_2O_2 on secreted proteins,
45 focusing on the oxidation of methionine (Met). Using the model white-rot model *Pycnoporus*
46 *cinnabarinus* grown on aspen wood, we showed that fungi protect their secreted proteins from
47 oxidation by reducing their Met content and utilizing a secreted catalase to scavenge exogenous
48 H_2O_2. The research identified key oxidizable Met within secreted CAZymes. Importantly, some Met
49 like those of GH7 cellobiohydrolases, undergone substantial oxidation levels suggesting important
50 roles in lignocellulose degradation. These findings highlight the adaptive mechanisms employed by
51 white-rot fungi to safeguard their secreted proteins during wood decay and emphasize the
52 importance of these processes in lignocellulose breakdown.

53

54 **Introduction**

55 Filamentous fungi are crucial in the carbon cycle because of their ability to decompose
56 organic matter and release carbon back into the ecosystem (1). Wood-decay fungi extract carbon
57 from recalcitrant polymers like cellulose and hemicelluloses embedded in a lignin matrix, by secreting
58 enzymes into the extracellular environment (2). The secreted proteins, commonly referred to as the
59 "secretome", contains the carbohydrate-active enzymes (CAZymes), including large sets of glycoside
60 hydrolases (GH) and auxiliary activity (AA) enzymes (3, 4). The GH class contains the endo- and exo-
61 acting enzymes targeting cellulose and hemicelluloses. The AA class contains laccases (AA1) and class
62 II peroxidases (AA2) involved in lignin degradation, and lytic polysaccharide monooxygenases (LPMO,
63 AA9) proposed to play an important role in the early phase of wood degradation (5–7). Reactive
64 oxygen species (ROS), particularly hydrogen peroxide (H_2O_2), play a crucial role in the early phase of
65 wood decay (8–10). H_2O_2 is generated by glucose-methanol-choline oxidoreductases (AA3) and
66 copper radical oxidases (AA5), that target carbohydrate or aliphatic/aromatic alcohols (11, 12). In
67 white-rot fungi, H_2O_2 acts as a co-substrate to fuel different types of LPMOs and AA2 peroxidases
68 (13–15). While the roles of CAZymes and H_2O_2 during the degradation of lignocellulose is well-
69 documented, the impact of ROS on the oxidation of CAZymes remains unclear. Fenton-generated
70 ROS were shown to decrease enzymatic activity of some GHs in white-rot secretomes, through the
71 oxidation of the secreted proteins, and the most abundant form of oxidation found was the oxidation
72 of Met residues (16). Met can be converted by H_2O_2 into Met sulfoxide (MetO) or Met sulfone
73 ($MetO_2$) and this has been shown to play critical roles in many organisms (17–20). For instance, Met
74 oxidation can lead either to a loss of function or act as a regulatory switch, to activate enzymes (21,
75 22). The presence of oxidizable Met in proteins can also be associated to an antioxidant role by
76 serving as a protection to avoid the oxidation of residues critical for the protein function (23). MetO
77 can be reduced back to Met by the methionine sulfoxide reductases, but, as these enzymes are most
78 likely not secreted, they cannot reduce oxidized Met of secreted proteins (24). Regarding the
79 importance of H_2O_2 during wood decay, our hypothesis is that some Met of secreted proteins can be

80 oxidized and play antioxidant or regulatory roles. Interestingly, the treatment of an α-galactosidase
81 (GH27) from *Trichoderma reesei* with H_2O_2 strongly increased its activity due to the oxidation of a
82 Met located near the active site, suggesting that Met oxidation of CAZymes can have a positive effect
83 on their activity (25). To identify secreted proteins with oxidizable Met, we selected the white-rot
84 *Pycnoporus cinnabarinus* grown on aspen wood as a model. *P. cinnabarinus* secretes H_2O_2-producing
85 enzymes in the early phase of wood degradation, to provide co-substrate for the H_2O_2-consuming
86 CAZymes (26), but also as potential oxidant of Met. We characterized the secreted proteins and
87 identified their oxidized Met with a redox proteomics approach using ^{18}O-labeled hydrogen peroxide
88 ($H_2{}^{18}O_2$) as a blocking reagent to prevent artifactual oxidation (27–30). Our investigations reveal the
89 extend of Met oxidation in fungal secretomes and the precise localization of oxidizable residues in
90 secreted proteins and CAZymes, suggesting potential antioxidant or regulatory roles.

91 **Results**

92 ***Secreted proteins retrieved by ion exchange chromatography are representative of early days***
93 ***decay.***

94 To identify oxidized Met in the secreted proteins during *P. cinnabarinus* growth, we focused
95 on the early days of wood decay, during which production and consumption of H_2O_2 are likely to
96 occur (26). We performed a time-course growth of the fungus on aspen wood and purified the
97 proteins from the culture supernatants at days 3, 5 and 7. To avoid artifactual oxidation that can
98 occur with standard methods combining a freezing step to protein concentration with ultrafiltration
99 (26, 31, 32), we purified the secreted proteins on successive anion and cation exchange
100 chromatography. Then, we oxidized the secreted proteins with $H_2{}^{18}O_2$ and identified them and their
101 potential oxidative Met modifications using proteomics (**Fig. S1**). We identified 308 secreted
102 proteins, among which CAZymes and proteases represented 41% and 10%, respectively (**Fig. 1; Table**
103 **1; Dataset 1**). Among the CAZymes, GH was by far the most represented class, with 89 proteins (71%)
104 spread over 34 families (**Fig. 1; Table 1**). We identified most of the CAZymes expected during wood
105 degradation, i.e. cellulases (GH3, GH5_5, GH5_9 and GH7, GH12, GH45), hemicellulases (GH10,
106 GH43, GH51, CE15, CE16) (4), as well as pectinases (GH28, CE8) and also some CAZymes targeting
107 fungal cell wall components (e.g. GH18 chitinases) (**Table 1**). Out of 23 identified AAs (18%), we
108 found laccases (AA1) and class II peroxidases (AA2), LPMOs (AA9) and H_2O_2-generating enzymes
109 (AA3, AA5). We estimated the abundance of the individual proteins using the Normalized Spectral
110 Abundance Factor (NSAF) (**Dataset 1**). The mean %NSAF of all identified proteins was ~ 0.3% and 52
111 proteins were above this value. The most abundant protein categories were CAZymes (52%), proteins
112 of unknown function (35%) and proteases (8%). Among the most abundant CAZymes, we found the
113 three cellobiohydrolases (GH7), three chitinases (GH18) and two laccases (AA1). Interestingly, three
114 H_2O_2-generating enzymes (two AA3_2 and one AA5_1) were among these most abundant CAZymes
115 (**Dataset 1**). Overall, the identity of the secreted proteins and their abundance were similar to those
116 previously described for *P. cinnabarinus* or very closely-related species (26, 31–33). This validates our

117 approach and indicates that the proteins preparation method and the oxidative treatment did not
118 affect the retrieval of the secreted proteins, and that they were suitable for studying Met sensitivity
119 to oxidation.
120

121 ***Met content is reduced in fungal secreted proteins.***

122 First, we evaluated the Met content of the secreted proteins, which was ~ 1.4% for each
123 time-point (**Fig. 2A**). Then, to determine whether some abundant proteins with specific Met content
124 could influence the overall content, we corrected the values by the proteins NSAF. The corrected Met
125 contents were 1.21 ± 0.02, 1.33 ± 0.02, and 1.35 ± 0.02, for days 3, 5, and 7, respectively, without
126 significant differences from the uncorrected values (**Fig. 2A**). These results indicate that the Met
127 content in the proteins secreted by *P. cinnabarinus* is comprised between 1.2 to 1.4%. Strikingly, this
128 value is twice lower than the general Met content of proteins, which is ~ 2.4% in average for all
129 protein sequences in the UniProt database (34). We investigated whether this characteristic may be
130 applied to all proteins predicted to be secreted. *P. cinnabarinus* has 666 proteins predicted to be
131 secreted with an average Met content of 1.55 ± 0.82%, while the non-secreted proteins have a higher
132 mean of 2.07 ± 0.96% Met. (**Fig. 2B; Table S1; Dataset 2**). These results show that *P. cinnabarinus*
133 secreted proteins contain significantly less Met than the non-secreted. Then, we compared the Met
134 content of experimentally validated secreted proteins from fungi, metazoans, and plants with the
135 Met content of intracellular proteins (**Fig. 2B; Table S1; Dataset 2**). The retrieved fungal secreted
136 proteins were almost exclusively from Dikarya (Ascomycota and Basidiomycota) and have a mean
137 Met content of 1.52 ± 0.74%, significantly lower than that of non-secreted proteins (2.17 ± 0.99%).
138 This decrease in Met content for secreted proteins is conserved when Ascomycota and
139 Basidiomycota are considered independently (**Fig. S2**). In contrast, the Met content of metazoans
140 secreted proteins (2.68 ± 1.40%) is significantly higher than that of the non-secreted proteins (2.41 ±
141 1.07%). No statistical difference exists between the Met content in secreted (2.59 ± 1.55%) and non-
142 secreted (2.55 ± 1.14%) proteins of plants (**Fig. 2B; Table S1; Dataset 2**). Altogether, these results

143 show that the secreted proteins of fungi contain less Met than the intracellular proteins, and that
144 this feature is not conserved in metazoans or plants.

145

146 ***A monofunctional catalase protects secreted proteins from oxidation.***

147 The identification of oxidizable Met in *P. cinnabarinus* secreted proteins required accurate
148 quantification of their oxidation levels. $H_2{}^{18}O_2$ was used to prevent artifactual Met oxidation
149 potentially occurring during sample preparation by blocking the Met reduced in the samples and
150 converting them to Met sulfoxide or sulfone containing ^{18}O atom (Met^{18}O and Met$^{18}O_2$, respectively).
151 The use of a concentrated $H_2{}^{18}O_2$ solution (100 mM) should allow the oxidation of all the reduced
152 Met and the reliable quantification of the initial levels of Met^{16}O and Met$^{16}O_2$ (28, 29). For the day 3
153 secretome, the levels of Met carrying ^{18}O or ^{16}O, either as sulfoxide or sulfone, were ~64% and
154 ~18%, respectively. Although ~18% of Met in reduced form was still present, this indicated that
155 most reduced Met in the culture conditions were blocked after the treatment with $H_2{}^{18}O_2$. Of note,
156 ^{16}O or ^{18}O sulfone levels reached ~2% (**Fig. 3A; Table S2; Dataset 3**). On the contrary, in day 5 and
157 day 7 secretomes, the levels of MetO and MetO_2 carrying ^{18}O were extremely low (~1%), indicating
158 that the blocking strategy failed for these samples (**Fig. 3A; Table S2; Dataset 3**). To evaluate
159 whether this lack of oxidation by $H_2{}^{18}O_2$ in secretomes of days 5 and 7 affected only Met residues, we
160 reanalyzed our data by searching for two main forms of Pro carbonylation bearing ^{18}O. For the day 3
161 secretome, we found slightly less than 4% of Pro oxidized with ^{18}O. A similar content of ^{16}O was
162 found, indicating that the large majority of Pro were not oxidized (~ 92%) (**Fig. 3B; Table S3; Dataset**
163 **4**). This low level of Pro oxidation was anticipated due to its low reactivity with $H_2{}^{18}O_2$ (35). The
164 percentage of ^{18}O oxidation decreased to ~0.5% in the day 5 and day 7 secretomes, while ^{16}O
165 oxidation levels remained comparable to those observed for the day 3 secretome. Thus, the trend for
166 Pro is the same as for Met indicating that the lack of oxidation observed for Met was not specific to
167 this residue. Proteins secreted during the days 5 and 7 of decay were not oxidized by exogenous

168 $H_2{}^{18}O_2$, unlike those secreted at day 3. These results prompted us to search for secreted enzymes
169 that scavenge H_2O_2. A catalase stood out: almost absent at day 3 (0.02 ± 0.02 %NSAF), but more
170 abundant at days 5 and 7, with %NSAF values of 0.33 ± 0.05 and 0.42 ± 0.01, respectively, above the
171 mean of ~ 0.3% found for all proteins (**Fig. 3C; Dataset 1**). When we measured the H_2O_2-consuming
172 activity of the secretomes, we observed no activity at day 3, but strong activities at days 5 and 7
173 secretomes, in a perfect consistency with the catalase abundance (**Fig. 3C**). Although a few potential
174 peroxidases and LPMOs were detected, their abundance was much lower than that of the catalase,
175 and none followed a similar trend over the three days (**Table S4; Dataset 1**). These results indicated
176 that this catalase was very likely responsible for most, if not all, of the H_2O_2-consuming activity. The
177 sequence and modeled structure analyses revealed that this secreted catalase is a typical
178 monofunctional catalase, similar to bacterial KatE enzymes or the peroxisomal enzyme found in
179 animals and yeast cells (36) (**Fig. S3**). Altogether, these results show that, under our experimental
180 conditions, *P. cinnabarinus* secreted a catalase at days 5 and 7, which, by consuming potential
181 exogenous H_2O_2, protected the secreted proteins from oxidation, whereas at day 3, the secreted
182 proteins are left without any protection against exogenous oxidant. Next, since Met oxidized with ^{18}O
183 were detected, we analyzed the nature of the oxidized proteins to identify Met residues with
184 potential antioxidant or regulatory roles.

185

186 ***Most of the oxidations occur on a few secreted CAZymes.***

187 Among the 308 secreted proteins identified, we detected 265 Met belonging to 118 proteins
188 (**Table S2; Dataset 3**). We selected only the Met-containing peptides present in all replicates for each
189 secretome, with at least five spectral counts, in at least two out of the three replicates. At day 3, all
190 selected Met were found to be oxidized with ^{18}O, at least partially (**Fig. 4A; Dataset 3**). The total
191 oxidation (^{16}O and ^{18}O) ranged from ~ 20% to 100% for the 46 identified Met (**Fig. 4A**). Four Met, all
192 from CAZymes, were fully oxidized and thus saturated with ^{18}O: Met305 of a PL35, Met378 of a GH7,

193 Met314 of a PL8, and Met239 of a CE16 (**Fig. 4A; Dataset 3**). Twenty-four proteins had oxidation
194 levels ranging from ~81% to 97% and 17 from 57% to ~80%. Only the Met592 from an AA3_2
195 displayed a much lower value of total oxidation (~20%) (**Fig. 4A; Dataset 3**). The ^{16}O-oxidation levels
196 were confidently evaluated for the four ^{18}O-saturated Met and should correspond to the levels
197 "naturally" found during the wood decay. However, for all other Met with an oxidation value less
198 than 100%, the saturation with ^{18}O was incomplete and some artifactual oxidation may have
199 occurred during the sample preparation, and thus the level of ^{16}O might be overestimated. For these
200 proteins, we assumed that the percentage of ^{16}O found during wood decay was necessarily equal to
201 or lower than the measured one. The percentage of oxidation as ^{16}O ranged from 0% to 47% with a
202 mean of 18% (**Fig. 4A; Dataset 3**). This value is consistent with the mean percentage of Met^{16}O
203 oxidation calculated considering all Met containing-peptides found (**see Fig. 3A**) and indicated that
204 most of the oxidation was concentrated on these few secreted proteins. Concerning day 5 and day 7
205 secretomes, the very low levels of ^{18}O oxidation precluded the use of the blocking strategy. However,
206 to find proteins with Met^{18}O may allow to consider $H_2{}^{18}O_2$ as a probe for highly reactive residues,
207 because of the low $H_2{}^{18}O_2$ concentration they were exposed to, due to the catalase activity. We
208 found eight and nine Met bearing ^{18}O in the proteins secreted at day 5 and day 7, respectively, and
209 five were common to both samples (**Fig. 4B; Dataset 3**). The percentages of ^{18}O ranged from ~2% to
210 ~14%, and from ~1% to ~23%, for the secreted proteins of day 5 and day 7, respectively. Among the
211 11 oxidized Met, only three were uniquely found at day 5 or day 7: Met533 of a GH95 at day 5, and
212 Met284 and Met160 belonging to a PL35 and a GH3, respectively, at day 7 (**Fig. 4B; Dataset 3**). This
213 indicates that most of the proteins found oxidized with ^{18}O at day 5 or 7 were also oxidized at day 3,
214 highlighting their high reactivity to H_2O_2. We found a total number of 49 oxidizable Met belonging to
215 28 proteins, representing ~24% and ~19% of all the identified Met and proteins from the secretome,
216 respectively (**Fig. 4C; Dataset 3**). Interestingly, the 18 identified CAZymes represented most of them
217 (64%), while proteases and proteins of unknown function both represented 18% with five identified
218 proteins. The most represented CAZymes were GHs with 10 identified proteins. These results

219 indicates that the proportion of oxidized CAZymes was enriched compared to the different types of
220 proteins present in the secretomes (**compare Fig. 4C with Fig. 1**).

221

222 ***Oxidation occurs in homologous proteins, at multiple sites and in hotspots.***

223 Interestingly, among the five most oxidized, three Met belong to the three GH7
224 (A0A060SFM6, A0A060SMU8, A0A060ST00, named A, B, and C, respectively), at position 286 of the
225 GH7 A and B, and at position 287 of the GH7 C (**Fig. 4A**). A sequence alignment showed that these
226 positions are conserved between these GH7 homologs (**Fig. 5A**). These Met were oxidized with
227 similar levels of $Met^{16}O$ (between 28% and 38%) and $Met^{16}O_2$ (between 9% and 13%). We also
228 detected seven other oxidized Met on these GH7s, four were uniquely on the GH7 A, one on the GH7
229 B, and two were in a position conserved in GH7 A and B. Since we had assessed the overall level of
230 Pro oxidation, we quantified the percentage of oxidation of individual Pro, considering only those
231 labeled with ^{18}O (**Dataset 4**). GH7 A had four oxidized Pro, two of which were in positions conserved
232 into the GH7 B (**Fig. 5A**). Interestingly, we found that oxidation of Met and/or Pro occurred on
233 homologs of GH16_2, PL35, proteases and GH152 (**Fig. 4; Fig. S4**). This represented 11 proteins
234 among the 33 proteins identified having oxidized residues (28 with Met with or without Pro and 5
235 with Pro only) (**Fig. 4; Fig. S4; Datasets 3; 4**). Moreover, 19 out of the 33 identified proteins were
236 oxidized on multiple residues, from two to 10. A GH152 was oxidized on 8 Pro, while the GH7 A was
237 the protein with the highest number of oxidation sites (10), including six Met and four Pro (**Fig. 4; Fig.
238 5; Fig. S4; Datasets 3; 4**). Finally, several oxidation sites were located close to each other in the
239 protein sequences, forming "hotspots" like the Pro343 and Met345, and three other Pro of the GH7
240 A (**Fig. 5A**). In total, we counted 24 occurrences of sites containing two oxidized residues in the
241 protein sequences (**Fig. 5B**). Analysis of a tridimensional model of GH7 A revealed that oxidized
242 residues distant on the sequence may be close on the structure, as the Met130 and Met160, the
243 Met153 in the vicinity of three Pro, and the Met286 clustered with the Pro343 and Met345 (**Fig. 5C**).

244 Altogether, these results indicate that most of the oxidation affects a relatively small set of CAZymes
245 that can be oxidized at multiple positions, with some hotspots. Moreover, the fact that oxidized
246 residues were found at similar positions within the homologs of *P. cinnabarinus* secreted proteins
247 suggests that these residues have been conserved to fulfill antioxidant or regulatory roles.

248

249 ***Conservation study suggests a list of residues with antioxidant or regulatory roles.***

250 To determine whether the 89 oxidized residues found in the 33 *P. cinnabarinus* proteins were
251 conserved in fungi, we searched for fungal homologs of the proteins and quantified the conservation
252 of the oxidized residues. Our hypothesis was that oxidizable residues playing antioxidant or
253 regulatory roles are more likely to be conserved among distantly related organisms, as shown for
254 Met of actin or of the ffh/SRP proteins (37–39). To avoid overrepresentation of sequences coming
255 from closely related organisms, the search was made in 120 representative fungal species, covering
256 the nine fungal phyla (**Dataset 5**). Overall, the conservation of Met or Pro ranged from 1% to 100%,
257 with a mean of 49%. Considering only residues with conservation values above 75%, and found in
258 more than 80 sequences, we obtained a list of nine Met and nine Pro at conserved positions in 14
259 secreted proteins (**Table 2**). The GH7 A has four conserved Met, among which Met 169 conserved in
260 99% of the homologs, and a conserved Pro. Other Met are conserved in the GH7 B and C, and in two
261 GH16_2, one GH18, one AA3_2 and a peptidase M36, present in all fungi (**Table 2; Dataset 5**).
262 Regarding Pro, three are conserved in all homologs, at positions 614, 143 and 441 of a GH16_2, a
263 GH28 and a laccase, respectively. Conserved Pro were also found in a AA3_2, an unknown protein
264 and a GH152 (**Table 2; Dataset 5**). These results allowed identification of proteins with oxidizable
265 Met and Pro residues strongly conserved across the fungal phyla.

266

267 **Discussion**

268 Taking a white-rot wood decayer as model, we showed that fungal secreted proteins have a
269 strongly reduced Met content (~1.4%) compared to the non-secreted (~2.1%) and that this feature
270 is not conserved in metazoans and plants. This reduced Met content could contribute to the
271 tolerance of the secreted enzymes to oxidation by reducing the number of sensitive residues. This
272 could explain, at least in part, the strong resistance of some CAZymes activities exposed to high
273 concentrations of Fenton-generated ROS observed in the brown-rot *Postia placenta* (16, 40).
274 Interestingly, these data contrast with those obtained from animal studies which showed that
275 proteins encoded by the mitochondrial genome may contain up to 6-10% Met. This high content
276 could act as an endogenous antioxidant with the exposed Met scavenging ROS which are then
277 removed by methionine sulfoxide reductases in a cycle of oxidation and reduction (41). A similar
278 mechanism was proposed in bacteria (42, 43). The absence of external system of MetO reduction
279 precludes the use of such mechanism with fungal secreted proteins (24). The protection of the
280 secreted proteins from oxidation is most likely also due to the activity of the secreted catalase we
281 identified (**Fig. 3; Table S4**), consistent with previous suggestions showing that the addition of
282 catalase to CAZymes cocktails reduces inactivation over time (44, 45). The secretion of a catalase by
283 *P. cinnabarinus* was unexpected, as it has not been previously detected in secretome analysis (26,
284 31). Moreover, catalase extracellular activity was also not measured for the white-rot *Phanerochaete*
285 *chrysosporium* (46). However, searching for secreted catalase homologs, we found that it is
286 widespread in Basidiomycota, and particularly in white-rot fungi (**Table S5**). This conclusion contrasts
287 with a previous phylogenetic analysis, which argued that Basidiomycota possess only monofunctional
288 catalases not predicted to be secreted because of the lack of a signal peptide (47). Lack of detection
289 of the protein or its activity may be due to specific expression conditions. In white-rot, it is surprising
290 that a catalase was expressed along with H_2O_2 producing and consuming enzymes. However,
291 catalases have Km values in the mM range (44), and their action could result in lowering the H_2O_2

292 concentration below a level that is damaging to proteins, but allows the activity of H_2O_2-driven
293 oxidoreductases.

294 Using $H_2{}^{18}O_2$-based proteomics, we identified oxidizable Met and highlighted that CAZymes were the
295 most oxidized secreted proteins during wood-decay, and that Met oxidation could occur on several
296 residues, sometimes clustered in hotspots. Clustering was also observed in bacterial proteins (48),
297 suggesting a universal phenomenon. The blocking strategy we used is based on a saturation of
298 reduced Met with ^{18}O. However, saturation was difficult to achieve, with only 4 Met saturated with
299 ^{18}O in the day 3 secretome (**Fig. 4**). An initial denaturation step would have probably allowed $H_2{}^{18}O_2$
300 to access the Met buried in the protein core (28). However, as our goal was to identify secreted
301 proteins with potential oxidizable Met we chose not to denature them. Our idea was that an
302 oxidizable Met should be accessible to an oxidant, either natural or $H_2{}^{18}O_2$. Indeed, the results at day
303 3 argue for the accessibility of Met since all identified Met but one carried both ^{16}O- and ^{18}O-
304 oxidation, with 43 Met out of 46 for which the percentage of ^{18}O was higher than that of ^{16}O. If a Met
305 would not have been accessible to an oxidant in the folded protein, the $H_2{}^{18}O_2$ would not have
306 oxidized it, and we could have observed ^{16}O, very likely coming from artifactual oxidation, but no ^{18}O.
307 However, as artefactual ^{16}O-oxidation cannot be totally ruled out, and potentially happened on the
308 remaining non-oxidized fraction of a considered Met during the proteomics procedure, we
309 considered that the "natural" percentage of ^{16}O was necessarily lower or equal to those measured. In
310 our study, the mean percentage of ^{16}O was 18%, while in studies on animals using similar
311 approaches, it was ~4% (27, 28), arguing for potential artifactual oxidation. However, while
312 intracellular proteins are protected by methionine sulfoxide reductases and ROS scavengers, the
313 MetO in secreted proteins cannot be reduced, and no H_2O_2-consuming was detected in the
314 secretome at day 3. Thus, to find high levels of MetO in fungal secreted proteins is expected.
315 Interestingly, nine Met were oxidized as ^{16}O sulfone among which five were also oxidized as Met$^{18}O_2$
316 (**Fig. 4**), confirming their propensity to form sulfone during wood decomposition.

317 Some of the Met we found oxidized in *P. cinnabarinus* are conserved throughout the fungal
318 kingdom, suggesting potentially important roles (**Table 5**). They could act as antioxidants, as for the
319 GH7 whose Met and Pro are located at the surface of the proteins and in the substrate cleft (**Fig. 5C**),
320 potentially preventing critical residues from being oxidized, as proposed for a glutamine synthetase
321 (23). Met sensitive to oxidation could also have a functional role altering enzyme activity like for a
322 GH18 in which a conserved oxidized Met is located near the catalytic residue (**Fig. S3**). This type of
323 regulation was shown for a GH27 galactosidase of *T. reesei*, for which Met oxidation increased
324 activity (25). In conclusion, our findings highlight a common mechanism in fungi preventing oxidation
325 of secreted proteins and, pinpoint redox-regulated CAZymes to be further characterized.

326

327 **Material and methods**

328 ***Culture of* P. cinnabarinus *on aspen wood.***

329 The dikaryotic strain *Pycnoporus cinnabarinus* CIRM-BRFM 145 was grown for 3, 5 or 7 days
330 at as described (26). The media contained maltose (2.5 g.l^{-1}) and *Populus tremuloides* aspen sawdust
331 particles of size < 2 mm (15 g. l^{-1}). Six replicates were mixed in pairs to obtain three replicate
332 samples per time-point.

333 ***Preparation of* P. cinnabarinus *secretomes and protein oxidation with $H_2{}^{18}O_2$.***

334 The culture supernatants containing the secreted proteins were centrifugated (1 h, 30,000xg,
335 10 °C) and sterilized by filtration (0.22 µm; Express Plus; Merck Millipore). The supernatants were
336 equilibrated to pH 7 with 0.5 mM NaOH and the proteins were purified using two ion exchange
337 chromatographies (**Fig. S1**): first, an anion exchange on DEAE Sephadex A-25 (Cytiva) and a cation
338 exchange on CM Sephadex A-25 (Cytiva) for proteins not retained on the anion exchanger. Both
339 resins were initially equilibrated with 20 mM sodium phosphate buffer (pH 7). Elution of the secreted
340 proteins was performed with 1 M NaCl. Fractions from both anion and cation exchangers were
341 pooled, desalted on Sephadex G-25 (PD-10 Desalting columns, Cytiva) in 50 mM sodium acetate (pH
342 5.2) and concentrated using Vivaspin polyethersulfone membrane (3 kDa cut-off, Sartorius). Protein
343 concentrations were determined using the Bradford method (Bio-Rad) and the secretomes were
344 used immediately. Secreted proteins (50 µg) were incubated 30 min with 1 mM hydroxylamine,
345 desalted on Sephadex G-25 (PD SpinTrap, Cytiva), then incubated with 100 mM of $H_2{}^{18}O_2$ (Sigma-
346 Aldrich) for 1 h in the dark, then desalted. Initial concentration of commercial $H_2{}^{18}O_2$ was estimated
347 to be ~ 450 mM using FOX method (49). Protein concentrations were determined, and the samples
348 were stored at -20°C.

349 ***Proteomics analysis.***

350 Proteins (15 µg) were precipitated by trichloroacetic acid and processed for trypsin
351 proteolysis as described (50). Peptides (5 µl) were injected into a nanoscale Easy-Spray™ PepMap™

352 Neo 2 µm C18 (75 µm x 750 mm) capillary column (Thermo Scientific) operated with a Vanquish Neo
353 UHPLC system (Thermo Scientific) and resolved with a 65-min gradient of CH_3CN (5-40%), 0.1%
354 formic acid, at a flow rate of 0.25 µL per min. Data-dependent acquisition analysis of the peptides
355 was performed with an Orbitrap Exploris 480 tandem mass spectrometer (Thermo) as described (51).
356 Each full scan of peptide ions in the high-field Orbitrap analyzer was acquired from m/z 350 to 1800
357 at a resolution of 120,000, selecting only 2+ and 3+ charged precursors for high-energy collisional
358 dissociation and with a dynamic exclusion of 10 seconds. MS/MS spectra of fragmented precursors
359 were acquired at a resolution of 15,000 and assigned to peptide sequences by the MASCOT Server
360 2.5.1 search engine (Matrix Science) using the *P. cinnabarinus* annotated proteome, with fixed and
361 variable modifications. Data are available in **Datasets 3; 4** of associated preprint (52). Proteins were
362 validated when at least two different peptides (p-value <0.01) were detected, resulting in a protein
363 identification false discovery rate below 1%. Protein abundance was estimated using the Normalized
364 Spectral Abundance Factor (NSAF) (53). The Met content of the proteins was calculated using the
365 entire sequence. The Met content corrected by the NSAF was calculated using the following formula:

$$\frac{\sum(\%Met_{protein\,n}\ X\ NSAF_{protein\,n})}{\sum NSAF_{protein\,n}}$$

366 With $\%Met_{protein\,n}$ and $NSAF_{protein\,n}$ corresponding to the percentage of Met and the NSAF value of the
367 individual proteins identified, respectively. The percentage of modification of Met or Pro residues
368 was calculated by dividing the number of spectral counts (SC) of the residue with the modification by
369 the total number of SC for the residue and then multiplying the result by 100. The mass spectrometry
370 proteomics data have been deposited to the ProteomeXchange Consortium via the PRIDE (54)
371 partner repository with the dataset identifier PXD046271 and 10.6019/PXD046271.

372

373 ***H_2O_2-consuming activity.***

374 Secreted proteins (20 µg) purified from day 3, 5 or 7 cultures as described before were
375 incubated with H_2O_2 (30 mM) for 1 h. Then, the proteins were removed from the samples by
376 ultrafiltration using Vivaspin 3 kDa cut-off and the filtrate was transferred into 1 ml quartz cuvette.
377 The residual H_2O_2 concentration in the filtrate was titrated by measuring the absorbance at 240 nm
378 using a molar extinction coefficient value of 43.6 $M^{-1}.cm^{-1}$ for H_2O_2. For each a day a control was
379 made incubating the H_2O_2 in the protein purification buffer without proteins. The experiment was
380 performed with a biological triplicate, and a technical duplicate. The activity of consumption was
381 calculated as follows:

$$H_2O_2\ consumption\ activity = \frac{[H_2O_2]_{in\ the\ control\ after\ 1h} - [H_2O_2]_{in\ the\ sample\ after\ 1h}}{Time\ of\ incubation\ \times\ Quantity\ of\ proteins}$$

382 ***Analysis of Met content in* P. cinnabarinus*, fungi, metazoans, and plants proteins.***

383 *P. cinnabarinus* proteins were predicted secreted if they fulfilled three conditions: (i)
384 presence of a secretion signal peptide, (ii) absence of endoplasmic reticulum retention motif and (iii)
385 absence of transmembrane helix outside the signal peptide, as described (26). Experimentally
386 validated fungal secreted proteins were retrieved from proteomics analyses (7, 26, 31–33, 55–65),
387 from Uniprot (www.uniprot.org) and FunSecKB2 (66). Metazoans experimentally validated secreted
388 were retrieved from Uniprot, MetazSecKB (67) and the Human Protein Atlas (68, 69). Experimentally
389 validated plant secreted proteins were retrieved from Uniprot, PlantSecKB (70) and the SUBA
390 database (71). The datasets of fungal, metazoans and plants non-secreted proteins were made using
391 proteins retrieved from Uniprot, the Human Protein Atlas and the SUBA database. For all datasets,
392 only manually curated proteins, and those found with least 5 SC in proteomics, were conserved.
393 Membrane proteins, proteins shorter than 50 amino acids, or not starting with Met were discarded.
394 Statistical analyses were unpaired t-test with Welch's correction. The numbers of proteins for each
395 category are described in **Table S1** and the protein sequences are available in **Datasets 2** (52).

396 ***Conservation of proteins and oxidized residues.***

397 A hundred and twenty fungal genomes were selected based on their public availability in the
398 MycoCosm database (72) and their representativity in the 9 fungal phyla (73, 74). Targets of the
399 oxidized proteins were searched using BLASTP (v 2.6.0+) (75). The 100 sequences with the highest e-
400 values were aligned using MAFFT tool (version 6.864b) (76). The conservation of individual residues
401 was made by counting its occurrence in all the sequences. Data are available in **Datasets 5** (52).

Acknowledgments

The authors kindly thank the CIRM-CF for providing the *P cinnabarinus* CIRM-BRFM145 strain, Dan Cullen (Forest Product Laboratory, USDA, Madison, WI, USA) for providing *Populus tremuloides* wood, and Marie-Noëlle Rosso (Aix Marseille Univ., INRAE, Biodiversité et Biotechnologies Fongiques) for critical reading of the manuscript. This work received support from the French government under the France 2030 investment plan, as part of the Initiative d'Excellence d'Aix-Marseille Université —IM2B (AMX-19-IET-006) for L.M. and L.T. – A*MIDEX (AMX-21-PEP-028) for L.T. The authors would like to thank the NovoNordisk foundation (OxyMiST project, grant number NNF20OC0059697) and the Commission Nationale des Outils Collectifs (CNOC) of INRAE for funding.

CRediT author statement

Lise Molinelli: Conceptualization, Methodology, Validation, Formal analysis, Investigation, Data Curation, Writing - Original Draft, Writing - Review & Editing, Visualization, **Elodie Drula:** Software, Methodology, Formal analysis, Investigation, Data Curation, **Jean-Charles Gaillard:** Formal analysis, Investigation, **David Navarro:** Investigation, Resources, **Jean Armengaud:** Formal analysis, Resources, Data Curation, Writing - Review & Editing, **Jean-Guy Berrin:** Resources, Writing - Review & Editing, Funding acquisition, **Thierry Tron:** Conceptualization, Resources, Writing - Review & Editing, Supervision, Funding acquisition, **Lionel Tarrago:** Conceptualization, Methodology, Software, Validation, Formal analysis, Investigation, Resources, Data Curation, Writing - Original Draft, Writing - Review & Editing, Visualization, Supervision, Funding acquisition.

424 **Figures legends**

425 **Figure 1. Distribution of the identified secreted proteins and CAZymes.** Values shown are the
426 aggregate of all replicates for each day (**Table 1; Dataset 1** (52)). Bar graphs represent the number of
427 CAZymes per class.

428 **Figure 2. Met content of *P. cinnabarinus* secreted proteins and comparison with fungal, metazoan,**
429 **and plant secreted and intracellular proteins. A)** The Met percentage of identified *P. cinnabarinus*
430 secreted proteins was calculated for each protein and averaged for the secretome of each day (*dark*
431 *blue* bars). Alternatively, the Met percentage for each protein was weighted by the protein NASF and
432 averaged *(light blue* bars). Values shown are the average of the 3 replicates ± standard deviation. **B)**
433 Met percentages of all proteins predicted to be secreted or intracellular in the *P. cinnabarinus* were
434 compared with the Met percentages of experimentally validated intracellular and secreted proteins
435 from fungi, metazoans, and plants (**Table 1; Dataset 1** (52)). Mean percentage of Met are indicated
436 with *black* lines. Statistical analysis was performed by unpaired t-test with Welch's correction
437 (****$P \leq 0.001$; *n.s.*, not significant).

438 **Figure 3. Levels of Met and Pro oxidation in the *P. cinnabarinus* secretomes and H_2O_2-consuming**
439 **activity. A)** Total levels of Met oxidation as sulfoxide and sulfone, either ^{16}O or ^{18}O calculated using
440 the spectral counts of all Met-containing peptides and compared to the level of non-oxidized Met for
441 each time point (**Table S2; Dataset 3** (52)). **B)** Total levels of Pro oxidation as glutamic 5-
442 semialdehyde (G5S) and pyroglutamic acid (PA), either ^{16}O or ^{18}O calculated using the spectral counts
443 of all Pro-containing peptides and compared to the level of non-oxidized Pro for each day (**Table S3;**
444 **Dataset 4** (52)). **C)** %NSAF of the catalase A0A060STN2 (**Dataset 1** (52)) and total H_2O_2-consuming
445 activity at each time point.

446 **Figure 4. Identity of oxidized Met and their levels of oxidation in *P. cinnabarinus* secretomes. A)**
447 Proportion of the different forms of oxidation for the Met identified in the secreted proteins at day 3.
448 Proteins are ranked based on the percentage of ^{16}O (MetO and $MetO_2$). The four Met fully oxidized

449 are underlined. Values shown are the mean of oxidation without standard deviation, omitted for
450 clarity. All values are in **Dataset 3** (52). **B)** Proportion of the different forms of oxidation for the Met
451 identified in the secreted proteins at day 5 and day 7. Proteins are ranked based on the percentage
452 of ^{18}O (MetO and $MetO_2$). All values are in **Dataset 3** (52). **C)** Distribution of the identified secreted
453 proteins and CAZymes with oxidized Met. Values shown are the aggregate of all replicates for each
454 time point (**Dataset 3** (52)). Bar graphs represent the number of CAZymes per class.

455 **Figure 5. Partial sequence alignment of GH7, numbers of oxidation sites and hotspots in identified**
456 **secreted proteins and tridimensional model of GH7. A**) Oxidized Met and Pro residues are on *blue*
457 and *orange* background, respectively. *Dark* and *light grey* backgrounds represent strictly conserved
458 and similar amino acids, respectively. Position and percentage of oxidation of the residues are
459 indicated above the sequence. For Pro, the percentage presented correspond to the sum of all
460 oxidized forms, either ^{16}O or ^{18}O at day 3, excepted the one indicated with 'D5', corresponding to Pro
461 oxidation at day 5. Underlined sequences represent peptides detected by LC-MS/MS. Accession
462 numbers are on the left of the sequences. **B**) Values correspond to the total number of oxidizable
463 Met and Pro sites found per protein. Hotspots correspond to the number of times that two oxidizable
464 sites were located within a window of ten amino acids on the protein sequence. All data are
465 presented in **Datasets 3** and **4** (52). **C**) 3D model of the GH7 A0A060SFM6 downloaded from
466 Alphafold database (77). The position of the cellonoanose substrate (in *blue*) was modelized using
467 the experimentally determined structure of *Trichoderma reesei* Cel7A (PDB #4C4C). Met and Pro
468 found oxidized are represented as *cyan* and *orange* sticks, respectively. Catalytic residues are
469 represented as *red* sticks. Percentage of oxidation at day 3 are in brackets. Some parts of the protein
470 were rendered transparent for clarity. Structure manipulation and image generation were done using
471 PyMol 2.3.2 (https://pymol.org/2/).

472

473 **Tables**

474 **Table 1. Number of identified secreted proteins.** The list of individual proteins and their abundance

475 is provided in the **Dataset 1** (52).

Type	*Day 3*	*Day 5*	*Day 7*	*Total count*	
Total proteins	212 ± 7	231 ± 7	225 ± 25	308	
Protease	21 ± 1	25 ± 2	23 ± 6	30	
Other	20 ± 3	21 ± 2	20 ± 2	35	
Unknown	72 ± 3	81 ± 3	78 ± 8	118	
CAZymes	99 ± 3	105 ± 4	104 ± 10	125	
Families					***Target substrate***
AA1_1; AA1_2	4 ± 0	4 ± 1	4 ± 0	5	Lignin; Iron
AA2	1 ± 0	2 ± 1	2 ± 2	5	Lignin
AA3_2	3 ± 0	3 ± 0	3 ± 0	4	Aryl-Alcohol/Glucose
AA5_1	3 ± 1	3 ± 0	3 ± 1	4	Glyoxal
AA8	1 ± 1	1 ± 0	0 ± 1	1	Iron
AA9	1 ±1	0 ± 1	1 ± 2	4	Cellulose
CBM1; CBM13; CBM50[a]	3 ± 0	3 ± 0	3 ± 0	3	Cellulose / Hemicellulose / Fungal cell wall
CE1	1 ± 0	1 ± 0	1 ± 0	1	Hemicellulose
CE4	1 ± 0	1 ± 0	1 ± 0	1	Hemicellulose
CE8	0 ± 1	1 ± 0	1 ± 1	1	Pectin
CE15	0 ± 1	1 ± 0	1 ± 0	1	Hemicellulose
CE16	2 ± 0	2 ± 0	2 ± 1	2	Hemicellulose
GH2	1 ± 0	1 ± 0	1 ± 0	1	Hemicellulose
GH3	3 ± 1	3 ± 0	3 ± 0	3	Cellulose
GH5_5; GH5_7; GH5_9	8 ± 1	9 ± 2	9 ± 1	11	Cellulose
GH7	3 ± 0	3 ± 0	3 ± 0	3	Cellulose
GH9	1 ± 1	1 ± 1	0 ± 1	1	Cellulose
GH10	4 ± 1	3 ± 1	4 ± 1	5	Hemicellulose
GH12	2 ± 0	1 ± 1	1 ± 1	2	Cellulose
GH13_1; GH13_32	2 ± 0	2 ± 1	2 ± 1	2	Starch
GH15	1 ± 0	1 ± 0	1 ± 0	1	Starch
GH16_1; GH16_2	9 ± 1	9 ± 0	9 ± 1	9	Hemicellulose / Unknown
GH17	2 ± 0	2 ± 0	2 ± 0	2	Hemicellulose
GH18	8 ± 0	8 ± 0	8 ± 1	10	Fungal cell wall
GH28	4 ± 1	4 ± 1	4 ± 0	5	Pectin
GH30_3	3 ± 0	2 ± 0	2 ± 0	3	Glycoproteins
GH31	2 ± 0	2 ± 0	2 ± 0	2	Glycoproteins
GH32	1 ± 0	1 ± 0	1 ± 0	1	Disaccharides
GH35	1 ± 0	1 ± 0	1 ± 0	1	Hemicellulose
GH37	1 ± 0	1 ± 0	1 ± 0	1	Disaccharides
GH43_6; GH43_24	1 ± 1	2 ± 0	2 ± 0	2	Hemicellulose
GH45	1 ± 0	1 ± 0	1 ± 0	1	Cellulose
GH47	1 ± 0	1 ± 0	1 ± 0	1	Hemicellulose
GH51	1 ± 0	1 ± 0	1 ± 0	1	Hemicellulose
GH55	2 ± 0	2 ± 0	2 ± 0	2	Hemicellulose
GH72	1 ± 0	1 ± 0	1 ± 0	1	Fungal cell wall
GH74	1 ± 0	1 ± 0	1 ± 0	1	Cellulose
GH76	2 ± 1	2 ± 1	2 ± 1	2	Glycoproteins
GH79	0 ± 1	2 ± 0	2 ± 0	2	Glycoproteins
GH88	n.d.	1 ± 0	1 ± 0		Pectin
GH92	1 ± 1	1 ± 0	1 ± 1	2	Glycoproteins
GH95	1 ± 0	1 ± 0	1 ± 0	1	Hemicellulose
GH125	0 ± 0	1 ± 0	1 ± 0	1	Fungal cell wall
GH128	2 ± 0	2 ± 0	1 ± 1	2	Fungal cell wall
GH131	2 ± 0	1 ± 1	2 ± 1	3	Cellulose
GH135	0 ± 1	1 ± 0	1 ± 0	1	Fungal cell wall
GH152	3 ± 0	3 ± 0	3 ± 0	3	Fungal cell wall
PL8_4	1 ± 0	1 ± 0	1 ± 0	1	Potentially Animals/Algae
PL14	1 ± 0	1 ± 0	1 ± 0	1	Potentially Animals/Algae

PL35	1 ± 0	1 ± 0	1 ± 0	2	Chondroitin
PL42	1 ± 0	1 ± 0	1 ± 0	1	Potentially Bacterial envelope

476 [a] *CBM* correspond to proteins for which only a CBM domain has been assigned. It should be noted

477 that other CAZymes possess a CBM associated with a catalytic domain. *n.d., not detected.*

478

479

480 **Table 2. *P. cinnabarinus* secreted proteins with oxidized residues conserved across fungal proteins.**

481 Only proteins for which the number of identified homolog sequences identified was higher than 80

482 were considered. The complete list of identified secreted proteins is presented in **Dataset 5** (52).

Accession Uniprot (JGI)	***Description***	***Repartition (Nb. of sequences)***	***Residue***	***Conservation (%)***
A0A060SFM6 (8640)	GH7	Dikarya (98)	Met 130	80
			Met 169	99
			Met 286[a]	76
			Met 378	83
			Pro 430[b]	99
A0A060ST00 (6809)	GH7	Dikarya (98)	Met 287[a]	76
			Pro 431[b]	99
A0A060SMU8 (5845)	GH7	Dikarya (98)	Met 286[a]	76
A0A060SIS0 (301)	GH16_2	Basidiomycota (100)	Met 615	92
			Pro 614	100
A0A060S933 (3097)	GH16_2	Basidiomycota (91)	Met 583	83
A0A060SC99 (6004)	GH18	Dikarya, Mucor., Zoo. (99)	Met 342	86
A0A060S4J1 (1984)	AA3_2	Agaricomycetes (100)	Met 124	83
A0A060SF78 (8374)	Pep. M36	All fungi (100)	Met 387	81
A0A060S2S5 (8001)	GH28	Dikarya (99)	Pro 143	100
Q9UVQ2 (8672)	Laccase	Basidiomycota (100)	Pro 284	96
			Pro 441	100
A0A060SC37 (3147)	AA3_2	Dikarya (98)	Pro 594	97
A0A060S4R6 (3419)	Unknown	Dikarya, Mucor., Chytridio., Neo. (100)	Pro 170	83
A0A060SF67 (3180)	GH152	Dikarya, Mucoromycota (99)	Pro 184[c]	94
A0A060SY89 (5455)	GH152	Dikarya, Mucor., Chytridio. (99)	Pro 200[c]	96

483 [a, b, c] Conserved positions between the *P. cinnabarinus* homologs. *Mucor., Mucoromycota; Zoo.,*

484 *Zoopagomycota, Chytridio., Chytridiomycota, Neo., Neocallimastigomycota.*

485

486 **References**

487 1. Fabian J, Zlatanovic S, Mutz M, Premke K. 2017. Fungal–bacterial dynamics and their
488 contribution to terrigenous carbon turnover in relation to organic matter quality. ISME J
489 11:415–425. https://doi.org/10.1038/ismej.2016.131

490 2. Baldrian P, Valášková V. 2008. Degradation of cellulose by basidiomycetous fungi. FEMS
491 Microbiol Rev 32:501–521. https://doi.org/10.1111/j.1574-6976.2008.00106.x

492 3. Drula E, Garron M-L, Dogan S, Lombard V, Henrissat B, Terrapon N. 2022. The carbohydrate-
493 active enzyme database: functions and literature. Nucleic Acids Res 50:D571–D577.
494 https://doi.org/10.1093/nar/gkab1045

495 4. Hage H, Rosso M-N. 2021. Evolution of Fungal Carbohydrate-Active Enzyme Portfolios and
496 Adaptation to Plant Cell-Wall Polymers. 3. J Fungi 7:185. https://doi.org/10.3390/jof7030185

497 5. Couturier M, Ladevèze S, Sulzenbacher G, Ciano L, Fanuel M, Moreau C, Villares A, Cathala B,
498 Chaspoul F, Frandsen KE, Labourel A, Herpoël-Gimbert I, Grisel S, Haon M, Lenfant N, Rogniaux
499 H, Ropartz D, Davies GJ, Rosso M-N, Walton PH, Henrissat B, Berrin J-G. 2018. Lytic xylan
500 oxidases from wood-decay fungi unlock biomass degradation. Nat Chem Biol 14:306–310.
501 https://doi.org/10.1038/nchembio.2558

502 6. Harris P V., Welner D, McFarland KC, Re E, Navarro Poulsen J-C, Brown K, Salbo R, Ding H,
503 Vlasenko E, Merino S, Xu F, Cherry J, Larsen S, Lo Leggio L. 2010. Stimulation of Lignocellulosic
504 Biomass Hydrolysis by Proteins of Glycoside Hydrolase Family 61: Structure and Function of a
505 Large, Enigmatic Family. Biochemistry 49:3305–3316. https://doi.org/10.1021/bi100009p

506 7. Navarro D, Rosso M-N, Haon M, Olivé C, Bonnin E, Lesage-Meessen L, Chevret D, Coutinho PM,
507 Henrissat B, Berrin J-G. 2014. Fast solubilization of recalcitrant cellulosic biomass by the

508 basidiomycete fungus *Laetisaria arvalis* involves successive secretion of oxidative and
509 hydrolytic enzymes. Biotechnol Biofuels 7:143. https://doi.org/10.1186/s13068-014-0143-5

510 8. Hori C, Gaskell J, Igarashi K, Kersten P, Mozuch M, Samejima M, Cullen D. 2014. Temporal
511 Alterations in the Secretome of the Selective Ligninolytic Fungus *Ceriporiopsis subvermispora*
512 during Growth on Aspen Wood Reveal This Organism's Strategy for Degrading Lignocellulose.
513 Appl Environ Microbiol 80:2062–2070. https://doi.org/10.1128/AEM.03652-13

514 9. Presley GN, Panisko E, Purvine SO, Schilling JS. 2018. Coupling secretomics with enzyme
515 activities to compare the temporal processes of wood metabolism among white and brown rot
516 fungi. Appl Environ Microbiol 84. https://doi.org/10.1128/AEM.00159-18

517 10. Zhang J, Presley GN, Hammel KE, Ryu J-S, Menke JR, Figueroa M, Hu D, Orr G, Schilling JS. 2016.
518 Localizing gene regulation reveals a staggered wood decay mechanism for the brown rot fungus
519 *Postia placenta*. Proc Natl Acad Sci 113:10968–10973.
520 https://doi.org/10.1073/pnas.1608454113

521 11. Cleveland ME, Mathieu Y, Ribeaucourt D, Haon M, Mulyk P, Hein JE, Lafond M, Berrin J-G,
522 Brumer H. 2021. A survey of substrate specificity among Auxiliary Activity Family 5 copper
523 radical oxidases. Cell Mol Life Sci CMLS 78:8187–8208. https://doi.org/10.1007/s00018-021-
524 03981-w

525 12. Sützl L, Laurent CVFP, Abrera AT, Schütz G, Ludwig R, Haltrich D. 2018. Multiplicity of enzymatic
526 functions in the CAZy AA3 family. Appl Microbiol Biotechnol 102:2477–2492.
527 https://doi.org/10.1007/s00253-018-8784-0

528 13. Bissaro B, Várnai A, Røhr ÅK, Eijsink VGH. 2018. Oxidoreductases and Reactive Oxygen Species
529 in Conversion of Lignocellulosic Biomass. Microbiol Mol Biol Rev 82:1–51.
530 https://doi.org/10.1128/mmbr.00029-18

531 14. Hiner ANP, Ruiz JH, López JNR, Cánovas FG, Brisset NC, Smith AT, Arnao MB, Acosta M. 2002.
532 Reactions of the Class II Peroxidases, Lignin Peroxidase and *Arthromyces ramosus* Peroxidase,
533 with Hydrogen Peroxide. J Biol Chem 277:26879–26885.
534 https://doi.org/10.1074/jbc.M200002200

535 15. Mattila H, Österman-Udd J, Mali T, Lundell T. 2022. Basidiomycota Fungi and ROS: Genomic
536 Perspective on Key Enzymes Involved in Generation and Mitigation of Reactive Oxygen Species.
537 Front Fungal Biol 3. https://doi.org/10.3389/ffunb.2022.837605

538 16. Castaño J, Zhang J, Zhou M, Tsai C-F, Lee JY, Nicora C, Schilling J. 2021. A Fungal Secretome
539 Adapted for Stress Enabled a Radical Wood Decay Mechanism. mBio
540 https://doi.org/10.1128/mBio.02040-21

541 17. Lim JM, Kim G, Levine RL. 2019. Methionine in Proteins: It's Not Just for Protein Initiation
542 Anymore. Neurochem Res 44:247–257. https://doi.org/10.1007/s11064-017-2460-0

543 18. Lourenço Dos Santos S, Petropoulos I, Friguet B. 2018. The Oxidized Protein Repair Enzymes
544 Methionine Sulfoxide Reductases and Their Roles in Protecting against Oxidative Stress, in
545 Ageing and in Regulating Protein Function. Antioxid Basel Switz 7:E191.
546 https://doi.org/10.3390/antiox7120191

547 19. Rey P, Tarrago L. 2018. Physiological Roles of Plant Methionine Sulfoxide Reductases in Redox
548 Homeostasis and Signaling. Antioxid Basel Switz 7:114. https://doi.org/10.3390/antiox7090114

549 20. Tarrago L, Kaya A, Kim H-Y, Manta B, Lee B-C, Gladyshev VN. 2022. The selenoprotein
550 methionine sulfoxide reductase B1 (MSRB1). Free Radic Biol Med 191:228–240.
551 https://doi.org/10.1016/j.freeradbiomed.2022.08.043

552 21. Erickson JR, Joiner M-LA, Guan X, Kutschke W, Yang J, Oddis C V, Bartlett RK, Lowe JS, O'Donnell
553 SE, Aykin-Burns N, Zimmerman MC, Zimmerman K, Ham A-JL, Weiss RM, Spitz DR, Shea MA,

554 Colbran RJ, Mohler PJ, Anderson ME. 2008. A Dynamic Pathway for Calcium-Independent
555 Activation of CaMKII by Methionine Oxidation. Cell 133:462–474.
556 https://doi.org/10.1016/j.cell.2008.02.048

557 22. Hou L, Kang I, Marchant RE, Zagorski MG. 2002. Methionine 35 Oxidation Reduces Fibril
558 Assembly of the Amyloid Aβ-(1–42) Peptide of Alzheimer's Disease *. J Biol Chem 277:40173–
559 40176. https://doi.org/10.1074/jbc.C200338200

560 23. Levine RL, Mosoni L, Berlett BS, Stadtman ER. 1996. Methionine residues as endogenous
561 antioxidants in proteins. Proc Natl Acad Sci U S A 93:15036–15040.
562 https://doi.org/10.1073/pnas.93.26.15036

563 24. Hage H, Rosso M-N, Tarrago L. 2021. Distribution of methionine sulfoxide reductases in fungi
564 and conservation of the free-methionine-R-sulfoxide reductase in multicellular eukaryotes. Free
565 Radic Biol Med 169:187–215. https://doi.org/10.1016/j.freeradbiomed.2021.04.013

566 25. Kachurin AM, Golubev AM, Geisow MM, Veselkina OS, Isaeva-Ivanova LS, Neustroev KN. 1995.
567 Role of methionine in the active site of α-galactosidase from *Trichoderma reesei*. Biochem J
568 308:955–964. https://doi.org/10.1042/bj3080955

569 26. Miyauchi S, Hage H, Drula E, Lesage-Meessen L, Berrin JG, Navarro D, Favel A, Chaduli D, Grisel
570 S, Haon M, Piumi F, Levasseur A, Lomascolo A, Ahrendt S, Barry K, LaButti KM, Chevret D, Daum
571 C, Mariette J, Klopp C, Cullen D, de Vries RP, Gathman AC, Hainaut M, Henrissat B, Hildén KS,
572 Kües U, Lilly W, Lipzen A, Mäkelä MR, Martinez AT, Morel-Rouhier M, Morin E, Pangilinan J,
573 Ram AFJ, Wösten HAB, Ruiz-Dueñas FJ, Riley R, Record E, Grigoriev I V., Rosso MN. 2020.
574 Conserved white-rot enzymatic mechanism for wood decay in the Basidiomycota genus
575 *Pycnoporus*. DNA Res Int J Rapid Publ Rep Genes Genomes 27:1–14.
576 https://doi.org/10.1093/dnares/dsaa011

577 27. Bettinger JQ, Simon M, Korotkov A, Welle KA, Hryhorenko JR, Seluanov A, Gorbunova V,
578 Ghaemmaghami S. 2022. Accurate Proteomewide Measurement of Methionine Oxidation in
579 Aging Mouse Brains. J Proteome Res 21:1495–1509.
580 https://doi.org/10.1021/acs.jproteome.2c00127

581 28. Bettinger JQ, Welle KA, Hryhorenko JR, Ghaemmaghami S. 2020. Quantitative Analysis of in
582 Vivo Methionine Oxidation of the Human Proteome. J Proteome Res 19:624–633.
583 https://doi.org/10.1021/acs.jproteome.9b00505

584 29. Liu H, Ponniah G, Neill A, Patel R, Andrien B. 2013. Accurate determination of protein
585 methionine oxidation by stable isotope labeling and LC-MS analysis. Anal Chem 85:11705–
586 11709. https://doi.org/10.1021/ac403072w

587 30. Shipman JT, Go EP, Desaire H. 2018. Method for Quantifying Oxidized Methionines and
588 Application to HIV-1 Env. J Am Soc Mass Spectrom 29:2041–2047.
589 https://doi.org/10.1007/s13361-018-2010-2

590 31. Levasseur A, Lomascolo A, Chabrol O, Ruiz-Dueñas FJ, Boukhris-Uzan E, Piumi F, Kües U, Ram
591 AFJ, Murat C, Haon M, Benoit I, Arfi Y, Chevret D, Drula E, Kwon MJ, Gouret P, Lesage-Meessen
592 L, Lombard V, Mariette J, Noirot C, Park J, Patyshakuliyeva A, Sigoillot JC, Wiebenga A, Wösten
593 HAB, Martin F, Coutinho PM, de Vries RP, Martínez AT, Klopp C, Pontarotti P, Henrissat B,
594 Record E. 2014. The genome of the white-rot fungus *Pycnoporus cinnabarinus*: a basidiomycete
595 model with a versatile arsenal for lignocellulosic biomass breakdown. BMC Genomics 15:486.
596 https://doi.org/10.1186/1471-2164-15-486

597 32. Miyauchi S, Navarro D, Grisel S, Chevret D, Berrin J-G, Rosso M-N. 2017. The integrative omics
598 of white-rot fungus Pycnoporus coccineus reveals co-regulated CAZymes for orchestrated
599 lignocellulose breakdown. PLoS ONE 12:e0175528.
600 https://doi.org/10.1371/journal.pone.0175528

601 33. Miyauchi S, Rancon A, Drula E, Hage H, Chaduli D, Favel A, Grisel S, Henrissat B, Herpoël-
602 Gimbert I, Ruiz-Dueñas FJ, Chevret D, Hainaut M, Lin J, Wang M, Pangilinan J, Lipzen A, Lesage-
603 Meessen L, Navarro D, Riley R, Grigoriev IV, Zhou S, Raouche S, Rosso M-N. 2018. Integrative
604 visual omics of the white-rot fungus *Polyporus brumalis* exposes the biotechnological potential
605 of its oxidative enzymes for delignifying raw plant biomass. Biotechnol Biofuels 11:201.
606 https://doi.org/10.1186/s13068-018-1198-5

607 34. UniProtKB/Swiss-Prot Release 2023_04 statistics.
608 https://web.expasy.org/docs/relnotes/relstat.html. Retrieved 14 September 2023.

609 35. Hawkins CL, Davies MJ. 2019. Detection, identification, and quantification of oxidative protein
610 modifications. J Biol Chem 294:19683–19708. https://doi.org/10.1074/jbc.REV119.006217

611 36. Zamocky M, Furtmüller PG, Obinger C. 2008. Evolution of Catalases from Bacteria to Humans.
612 Antioxid Redox Signal 10:1527–1548. https://doi.org/10.1089/ars.2008.2046

613 37. Ezraty B, Grimaud R, El Hassouni M, Moinier D, Barras F. 2004. Methionine sulfoxide reductases
614 protect Ffh from oxidative damages in *Escherichia coli*. EMBO J 23:1868–1877.
615 https://doi.org/10.1038/sj.emboj.7600172

616 38. Laugier E, Tarrago L, Vieira Dos Santos C, Eymery F, Havaux M, Rey P. 2010. *Arabidopsis*
617 *thaliana* plastidial methionine sulfoxide reductases B, MSRBs, account for most leaf peptide
618 MSR activity and are essential for growth under environmental constraints through a role in the
619 preservation of photosystem antennae. Plant J Cell Mol Biol 61:271–282.
620 https://doi.org/10.1111/j.1365-313X.2009.04053.x

621 39. Rouyère C, Serrano T, Frémont S, Echard A. 2022. Oxidation and reduction of actin: Origin,
622 impact in vitro and functional consequences in vivo. Eur J Cell Biol 101:151249.
623 https://doi.org/10.1016/j.ejcb.2022.151249

624 40. Castaño JD, Zhang J, Anderson CE, Schilling JS. 2018. Oxidative Damage Control during Decay of
625 Wood by Brown Rot Fungus Using Oxygen Radicals. Appl Environ Microbiol 84:e01937-18.
626 https://doi.org/10.1128/AEM.01937-18

627 41. Bender A, Hajieva P, Moosmann B. 2008. Adaptive antioxidant methionine accumulation in
628 respiratory chain complexes explains the use of a deviant genetic code in mitochondria. Proc
629 Natl Acad Sci U S A 105:16496–16501. https://doi.org/10.1073/pnas.0802779105

630 42. Melnyk RA, Youngblut MD, Clark IC, Carlson HK, Wetmore KM, Price MN, Iavarone AT,
631 Deutschbauer AM, Arkin AP, Coates JD. 2015. Novel mechanism for scavenging of hypochlorite
632 involving a periplasmic methionine-rich Peptide and methionine sulfoxide reductase. mBio
633 6:e00233-00215. https://doi.org/10.1128/mBio.00233-15

634 43. Luo S, Levine RL. 2009. Methionine in proteins defends against oxidative stress. FASEB J Off
635 Publ Fed Am Soc Exp Biol 23:464–472. https://doi.org/10.1096/fj.08-118414

636 44. Peciulyte A, Samuelsson L, Olsson L, McFarland KC, Frickmann J, Østergård L, Halvorsen R, Scott
637 BR, Johansen KS. 2018. Redox processes acidify and decarboxylate steam-pretreated
638 lignocellulosic biomass and are modulated by LPMO and catalase. Biotechnol Biofuels 11:165.
639 https://doi.org/10.1186/s13068-018-1159-z

640 45. Scott BR, Huang HZ, Frickman J, Halvorsen R, Johansen KS. 2016. Catalase improves
641 saccharification of lignocellulose by reducing lytic polysaccharide monooxygenase-associated
642 enzyme inactivation. Biotechnol Lett 38:425–434. https://doi.org/10.1007/s10529-015-1989-8

643 46. Kwon S-I, Anderson AJ. 2001. Catalase Activities of Phanerochaete chrysosporium Are Not
644 Coordinately Produced with Ligninolytic Metabolism: Catalases from a White-Rot Fungus. Curr
645 Microbiol 42:8–11. https://doi.org/10.1007/s002840010169

646 47. Hansberg W, Salas-Lizana R, Domínguez L. 2012. Fungal catalases: function, phylogenetic origin
647 and structure. Arch Biochem Biophys 525:170–180. https://doi.org/10.1016/j.abb.2012.05.014

648 48. Tarrago L, Grosse S, Siponen MI, Lemaire D, Alonso B, Miotello G, Armengaud J, Arnoux P,
649 Pignol D, Sabaty M. 2018. *Rhodobacter sphaeroides* methionine sulfoxide reductase P reduces
650 R- and S-diastereomers of methionine sulfoxide from a broad-spectrum of protein substrates.
651 Biochem J 475:3779–3795. https://doi.org/10.1042/BCJ20180706

652 49. Wolff SP. 1994. [18] Ferrous ion oxidation in presence of ferric ion indicator xylenol orange for
653 measurement of hydroperoxides, p. 182–189. *In* Methods in Enzymology. Academic Press.
654 https://doi.org/10.1016/S0076-6879(94)33021-2

655 50. Hartmann EM, Allain F, Gaillard J-C, Pible O, Armengaud J. 2014. Taking the shortcut for high-
656 throughput shotgun proteomic analysis of bacteria. Methods Mol Biol Clifton NJ 1197:275–285.
657 https://doi.org/10.1007/978-1-4939-1261-2_16

658 51. Lozano C, Grenga L, Gallais F, Miotello G, Bellanger L, Armengaud J. 2023. Mass spectrometry
659 detection of monkeypox virus: Comprehensive coverage for ranking the most responsive
660 peptide markers. Proteomics 23:e2200253. https://doi.org/10.1002/pmic.202200253

661 52. Molinelli L, Drula E, Gaillard J-C, Navarro D, Armengaud J, Berrin J-G, Tron T, Tarrago L. 2023.
662 Methionine oxidation of Carbohydrate-Active enZymes during white-rot wood decay. bioRxiv
663 https://doi.org/10.1101/2023.10.24.563746

664 53. Paoletti AC, Parmely TJ, Tomomori-Sato C, Sato S, Zhu D, Conaway RC, Conaway JW, Florens L,
665 Washburn MP. 2006. Quantitative proteomic analysis of distinct mammalian Mediator
666 complexes using normalized spectral abundance factors. Proc Natl Acad Sci 103:18928–18933.
667 https://doi.org/10.1073/pnas.0606379103

668 54. Perez-Riverol Y, Bai J, Bandla C, García-Seisdedos D, Hewapathirana S, Kamatchinathan S,
669 Kundu DJ, Prakash A, Frericks-Zipper A, Eisenacher M, Walzer M, Wang S, Brazma A, Vizcaíno
670 JA. 2021. The PRIDE database resources in 2022: a hub for mass spectrometry-based
671 proteomics evidences. Nucleic Acids Res 50:D543–D552. https://doi.org/10.1093/nar/gkab1038

672 55. Arfi Y, Chevret D, Henrissat B, Berrin J-G, Levasseur A, Record E. 2013. Characterization of salt-
673 adapted secreted lignocellulolytic enzymes from the mangrove fungus *Pestalotiopsis* sp. Nat
674 Commun 4:1810. https://doi.org/10.1038/ncomms2850

675 56. Arntzen MØ, Bengtsson O, Várnai A, Delogu F, Mathiesen G, Eijsink VGH. 2020. Quantitative
676 comparison of the biomass-degrading enzyme repertoires of five filamentous fungi. Sci Rep
677 10:20267. https://doi.org/10.1038/s41598-020-75217-z

678 57. Couturier M, Navarro D, Chevret D, Henrissat B, Piumi F, Ruiz-Dueñas FJ, Martinez AT, Grigoriev
679 IV, Riley R, Lipzen A, Berrin J-G, Master ER, Rosso M-N. 2015. Enhanced degradation of
680 softwood versus hardwood by the white-rot fungus *Pycnoporus coccineus*. Biotechnol Biofuels
681 8:216. https://doi.org/10.1186/s13068-015-0407-8

682 58. Couturier M, Navarro D, Olivé C, Chevret D, Haon M, Favel A, Lesage-Meessen L, Henrissat B,
683 Coutinho PM, Berrin J-G. 2012. Post-genomic analyses of fungal lignocellulosic biomass
684 degradation reveal the unexpected potential of the plant pathogen *Ustilago maydis*. BMC
685 Genomics 13:57. https://doi.org/10.1186/1471-2164-13-57

686 59. Daou M, Farfan Soto C, Majira A, Cézard L, Cottyn B, Pion F, Navarro D, Oliveira Correia L, Drula
687 E, Record E, Raouche S, Baumberger S, Faulds CB. 2021. Fungal Treatment for the Valorization
688 of Technical Soda Lignin. J Fungi Basel Switz 7:39. https://doi.org/10.3390/jof7010039

689 60. Filiatrault-Chastel C, Navarro D, Haon M, Grisel S, Herpoël-Gimbert I, Chevret D, Fanuel M,
690 Henrissat B, Heiss-Blanquet S, Margeot A, Berrin J-G. 2019. AA16, a new lytic polysaccharide

691 monooxygenase family identified in fungal secretomes. Biotechnol Biofuels 12:55.
692 https://doi.org/10.1186/s13068-019-1394-y

693 61. Miyauchi S, Navarro D, Grigoriev IV, Lipzen A, Riley R, Chevret D, Grisel S, Berrin J-G, Henrissat
694 B, Rosso M-N. 2016. Visual Comparative Omics of Fungi for Plant Biomass Deconstruction. Front
695 Microbiol 7. https://doi.org/10.3389/fmicb.2016.01335

696 62. Paës G, Navarro D, Benoit Y, Blanquet S, Chabbert B, Chaussepied B, Coutinho PM, Durand S,
697 Grigoriev IV, Haon M, Heux L, Launay C, Margeot A, Nishiyama Y, Raouche S, Rosso M-N, Bonnin
698 E, Berrin J-G. 2019. Tracking of enzymatic biomass deconstruction by fungal secretomes
699 highlights markers of lignocellulose recalcitrance. Biotechnol Biofuels 12:76.
700 https://doi.org/10.1186/s13068-019-1417-8

701 63. Poidevin L, Berrin J-G, Bennati-Granier C, Levasseur A, Herpoël-Gimbert I, Chevret D, Coutinho
702 PM, Henrissat B, Heiss-Blanquet S, Record E. 2014. Comparative analyses of *Podospora*
703 *anserina* secretomes reveal a large array of lignocellulose-active enzymes. Appl Microbiol
704 Biotechnol 98:7457–7469. https://doi.org/10.1007/s00253-014-5698-3

705 64. Reyre J-L, Grisel S, Haon M, Navarro D, Ropartz D, Le Gall S, Record E, Sciara G, Tranquet O,
706 Berrin J-G, Bissaro B. 2022. The Maize Pathogen *Ustilago maydis* Secretes Glycoside Hydrolases
707 and Carbohydrate Oxidases Directed toward Components of the Fungal Cell Wall. Appl Environ
708 Microbiol 88:e0158122. https://doi.org/10.1128/aem.01581-22

709 65. Ribeaucourt D, Saker S, Navarro D, Bissaro B, Drula E, Correia LO, Haon M, Grisel S, Lapalu N,
710 Henrissat B, O'Connell RJ, Lambert F, Lafond M, Berrin J-G. 2021. Identification of Copper-
711 Containing Oxidoreductases in the Secretomes of Three *Colletotrichum* Species with a Focus on
712 Copper Radical Oxidases for the Biocatalytic Production of Fatty Aldehydes. Appl Environ
713 Microbiol 87:e0152621. https://doi.org/10.1128/AEM.01526-21

714 66. Meinken J, Asch DK, Neizer-Ashun KA, Chang G-H, R.Cooper JR C, Min XJ. 2014. FunSecKB2: a
715 fungal protein subcellular location knowledgebase. Comput Mol Biol
716 https://doi.org/10.5376/CMB.2014.04.0007

717 67. Meinken J, Walker G, Cooper CR, Min XJ. 2015. MetazSecKB: the human and animal secretome
718 and subcellular proteome knowledgebase. Database 2015:1–14.
719 https://doi.org/10.1093/database/bav077

720 68. Uhlén M, Fagerberg L, Hallström BM, Lindskog C, Oksvold P, Mardinoglu A, Sivertsson Å, Kampf
721 C, Sjöstedt E, Asplund A, Olsson IM, Edlund K, Lundberg E, Navani S, Szigyarto CAK, Odeberg J,
722 Djureinovic D, Takanen JO, Hober S, Alm T, Edqvist PH, Berling H, Tegel H, Mulder J, Rockberg J,
723 Nilsson P, Schwenk JM, Hamsten M, Von Feilitzen K, Forsberg M, Persson L, Johansson F,
724 Zwahlen M, Von Heijne G, Nielsen J, Pontén F. 2015. Tissue-based map of the human
725 proteome. Science 347. https://doi.org/10.1126/science.1260419

726 69. Uhlén M, Karlsson MJ, Hober A, Svensson AS, Scheffel J, Kotol D, Zhong W, Tebani A, Strandberg
727 L, Edfors F, Sjöstedt E, Mulder J, Mardinoglu A, Berling A, Ekblad S, Dannemeyer M, Kanje S,
728 Rockberg J, Lundqvist M, Malm M, Volk AL, Nilsson P, Månberg A, Dodig-Crnkovic T, Pin E,
729 Zwahlen M, Oksvold P, von Feilitzen K, Häussler RS, Hong MG, Lindskog C, Ponten F, Katona B,
730 Vuu J, Lindström E, Nielsen J, Robinson J, Ayoglu B, Mahdessian D, Sullivan D, Thul P, Danielsson
731 F, Stadler C, Lundberg E, Bergström G, Gummesson A, Voldborg BG, Tegel H, Hober S,
732 Forsström B, Schwenk JM, Fagerberg L, Sivertsson Å. 2019. The human secretome. Sci Signal 12.
733 https://doi.org/10.1126/scisignal.aaz0274

734 70. Lum G, Meinken J, Orr J, Frazier S, Min XJ. 2014. PlantSecKB: the Plant Secretome and
735 Subcellular Proteome KnowledgeBase. Comput Mol Biol 4.
736 https://doi.org/10.5376/cmb.2014.04.0001

737 71. Hooper CM, Castleden IR, Tanz SK, Aryamanesh N, Millar AH. 2017. SUBA4: the interactive data
738 analysis centre for Arabidopsis subcellular protein locations. Nucleic Acids Res 45:D1064–
739 D1074. https://doi.org/10.1093/nar/gkw1041

740 72. Grigoriev IV, Nikitin R, Haridas S, Kuo A, Ohm R, Otillar R, Riley R, Salamov A, Zhao X,
741 Korzeniewski F, Smirnova T, Nordberg H, Dubchak I, Shabalov I. 2014. MycoCosm portal:
742 gearing up for 1000 fungal genomes. Nucleic Acids Res 42:D699–D704.
743 https://doi.org/10.1093/nar/gkt1183

744 73. Zhao Z, Liu H, Wang C, Xu JR. 2014. Correction to Comparative analysis of fungal genomes
745 reveals different plant cell wall degrading capacity in fungi [BMC Genomics 14(2013) 274]. BMC
746 Genomics 15:1–15. https://doi.org/10.1186/1471-2164-15-6

747 74. Miyauchi S, Kiss E, Kuo A, Drula E, Kohler A, Sánchez-García M, Morin E, Andreopoulos B, Barry
748 KW, Bonito G, Buée M, Carver A, Chen C, Cichocki N, Clum A, Culley D, Crous PW, Fauchery L,
749 Girlanda M, Hayes RD, Kéri Z, LaButti K, Lipzen A, Lombard V, Magnuson J, Maillard F, Murat C,
750 Nolan M, Ohm RA, Pangilinan J, Pereira M de F, Perotto S, Peter M, Pfister S, Riley R, Sitrit Y,
751 Stielow JB, Szöllősi G, Žifčáková L, Štursová M, Spatafora JW, Tedersoo L, Vaario L-M, Yamada A,
752 Yan M, Wang P, Xu J, Bruns T, Baldrian P, Vilgalys R, Dunand C, Henrissat B, Grigoriev I V.,
753 Hibbett D, Nagy LG, Martin FM. 2020. Large-scale genome sequencing of mycorrhizal fungi
754 provides insights into the early evolution of symbiotic traits. Nat Commun 11:5125.
755 https://doi.org/10.1038/s41467-020-18795-w

756 75. Camacho C, Coulouris G, Avagyan V, Ma N, Papadopoulos J, Bealer K, Madden TL. 2009.
757 BLAST+: architecture and applications. BMC Bioinformatics 10:421.
758 https://doi.org/10.1186/1471-2105-10-421

759 76. Katoh K, Rozewicki J, Yamada KD. 2019. MAFFT online service: multiple sequence alignment,
760 interactive sequence choice and visualization. Brief Bioinform 20:1160–1166.
761 https://doi.org/10.1093/bib/bbx108

762 77. Varadi M, Anyango S, Deshpande M, Nair S, Natassia C, Yordanova G, Yuan D, Stroe O, Wood G,
763 Laydon A, Žídek A, Green T, Tunyasuvunakool K, Petersen S, Jumper J, Clancy E, Green R, Vora
764 A, Lutfi M, Figurnov M, Cowie A, Hobbs N, Kohli P, Kleywegt G, Birney E, Hassabis D, Velankar S.
765 2022. AlphaFold Protein Structure Database: massively expanding the structural coverage of
766 protein-sequence space with high-accuracy models. Nucleic Acids Res 50:D439–D444.
767 https://doi.org/10.1093/nar/gkab1061

768

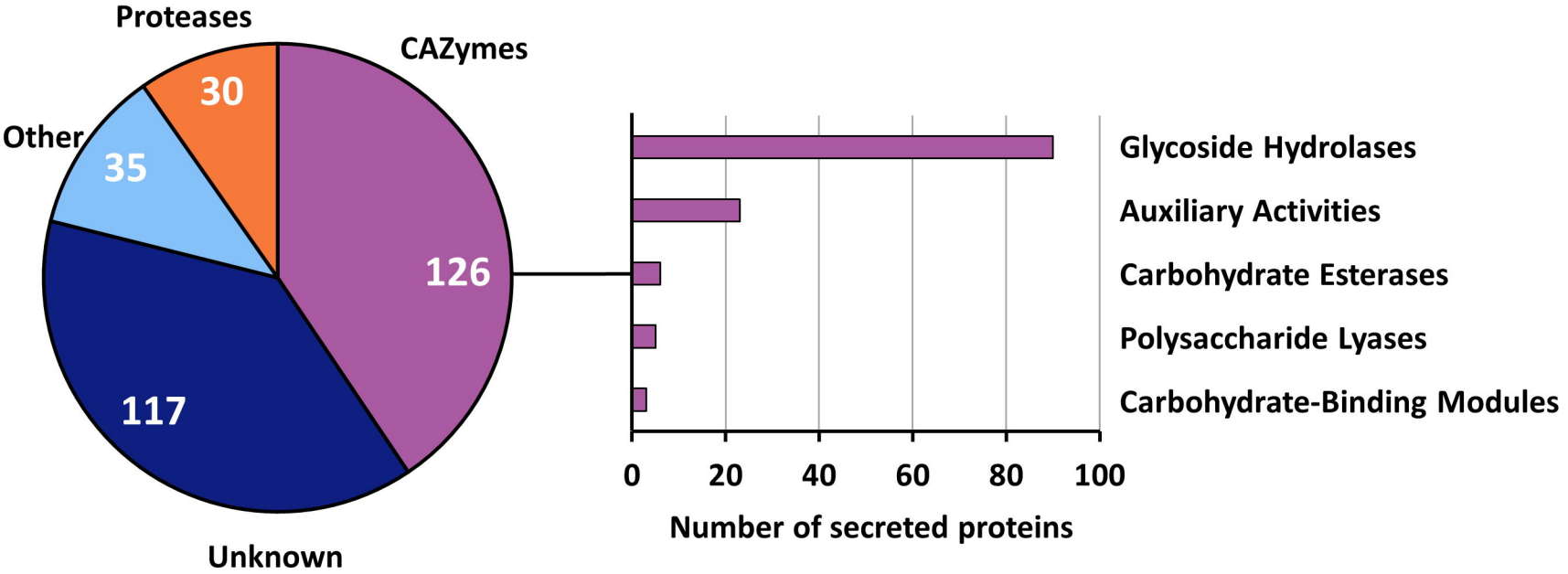
Proteases
CAZymes
Other
30
35
126
117
Unknown
Glycoside Hydrolases
Auxiliary Activities
Carbohydrate Esterases
Polysaccharide Lyases
Carbohydrate-Binding Modules
0
20
40
60
80
100
Number of secreted proteins

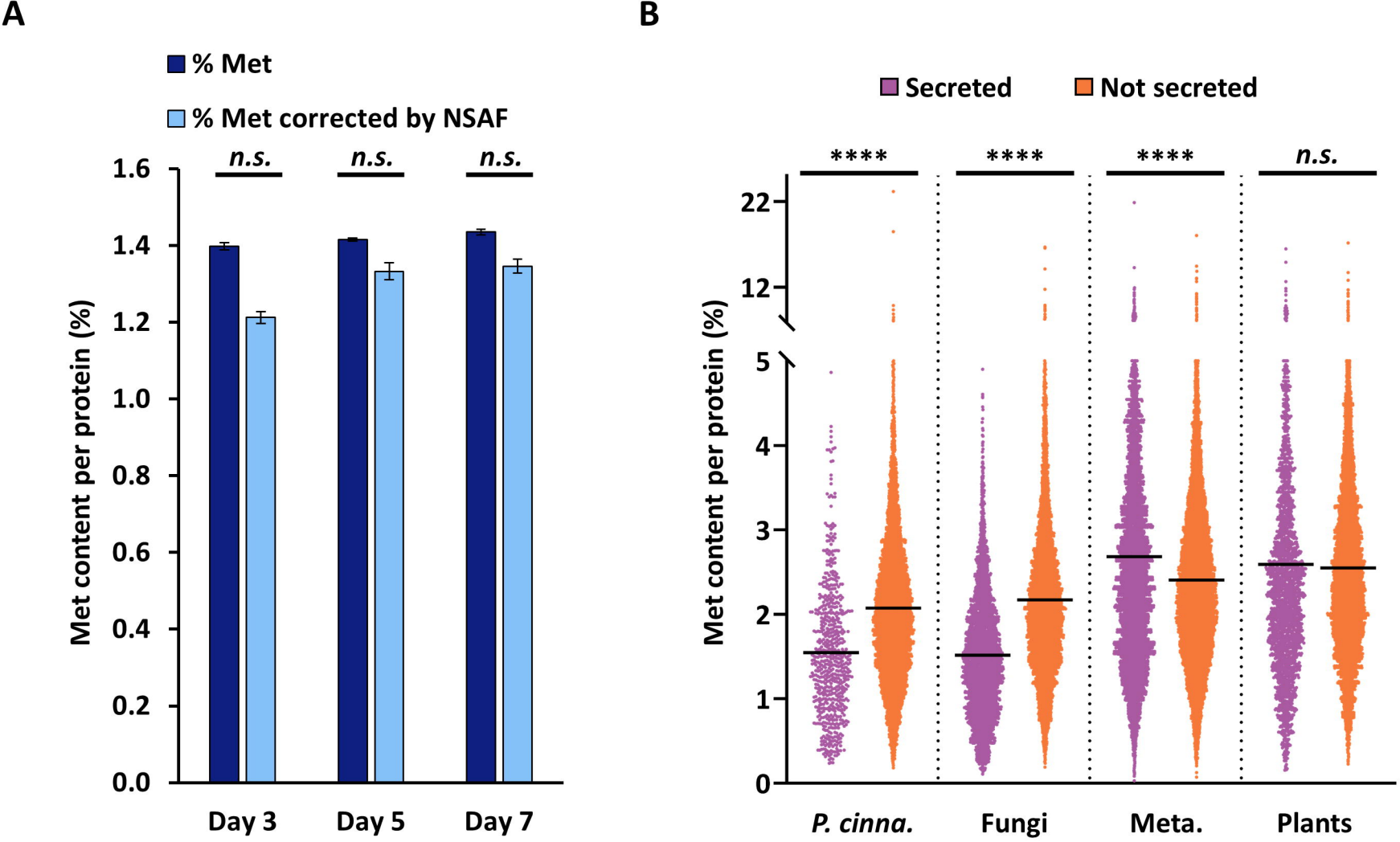
A
% Met
% Met corrected by NSAF
n.s.
n.s.
n.s.
Met content per protein (%)
1.6
1.4
1.2
1.0
0.8
0.6
0.4
0.2
0.0
Day 3
Day 5
Day 7
B
Secreted
Not secreted
****
****
****
n.s.
Met content per protein (%)
22
12
5
4
3
2
1
0
P. cinna.
Fungi
Meta.
Plants

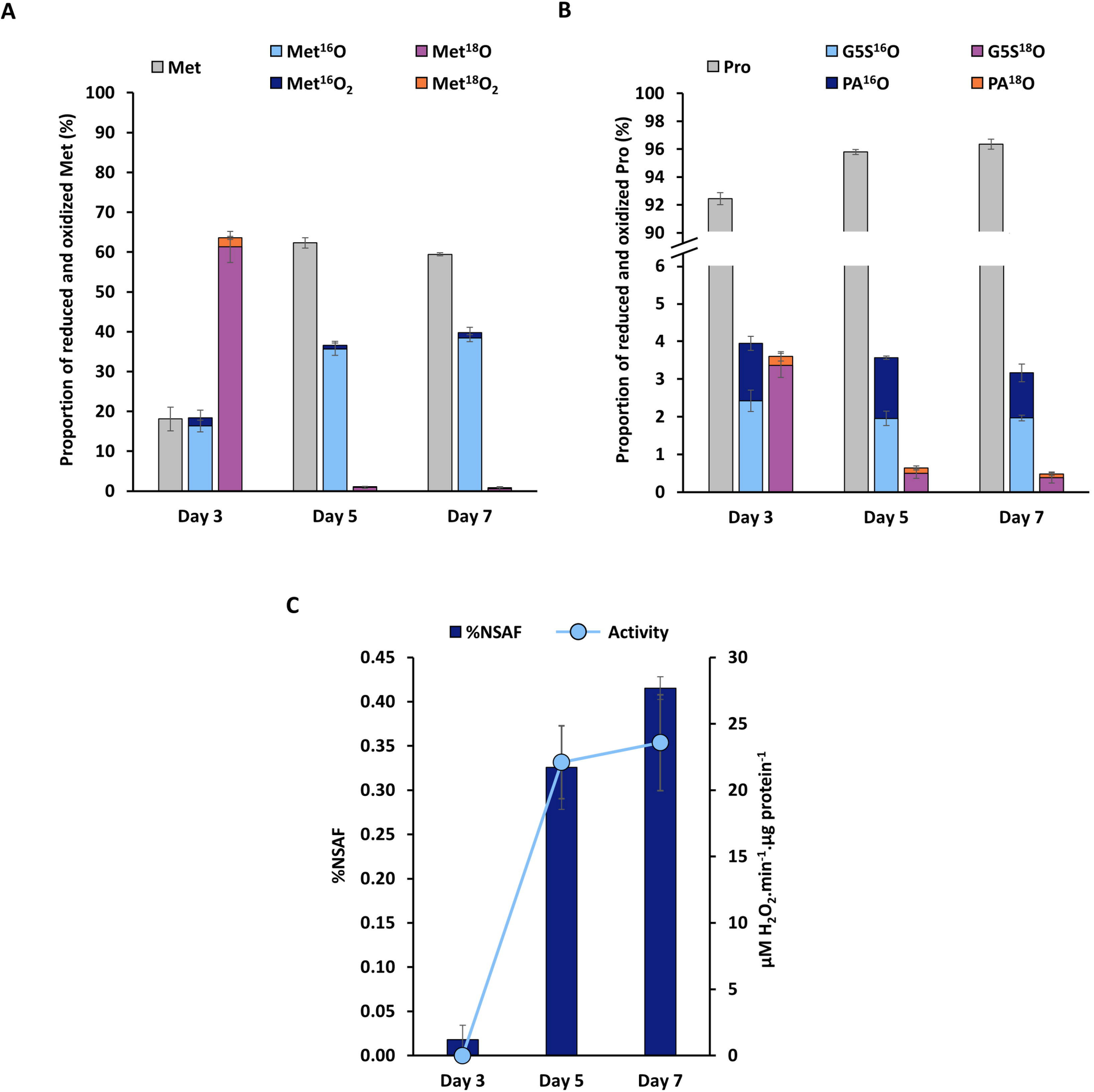
A
Met
Met16O
Met18O
Met16O2
Met18O2
Proportion of reduced and oxidized Met (%)
100
90
80
70
60
50
40
30
20
10
0
Day 3
Day 5
Day 7
B
Pro
G5S16O
G5S18O
PA16O
PA18O
Proportion of reduced and oxidized Pro (%)
100
98
96
94
92
90
6
5
4
3
2
1
0
Day 3
Day 5
Day 7
C
%NSAF
Activity
0.45
0.40
0.35
0.30
0.25
0.20
0.15
0.10
0.05
0.00
30
25
20
15
10
5
0
μM H2O2.min-1.μg protein-1
Day 3
Day 5
Day 7

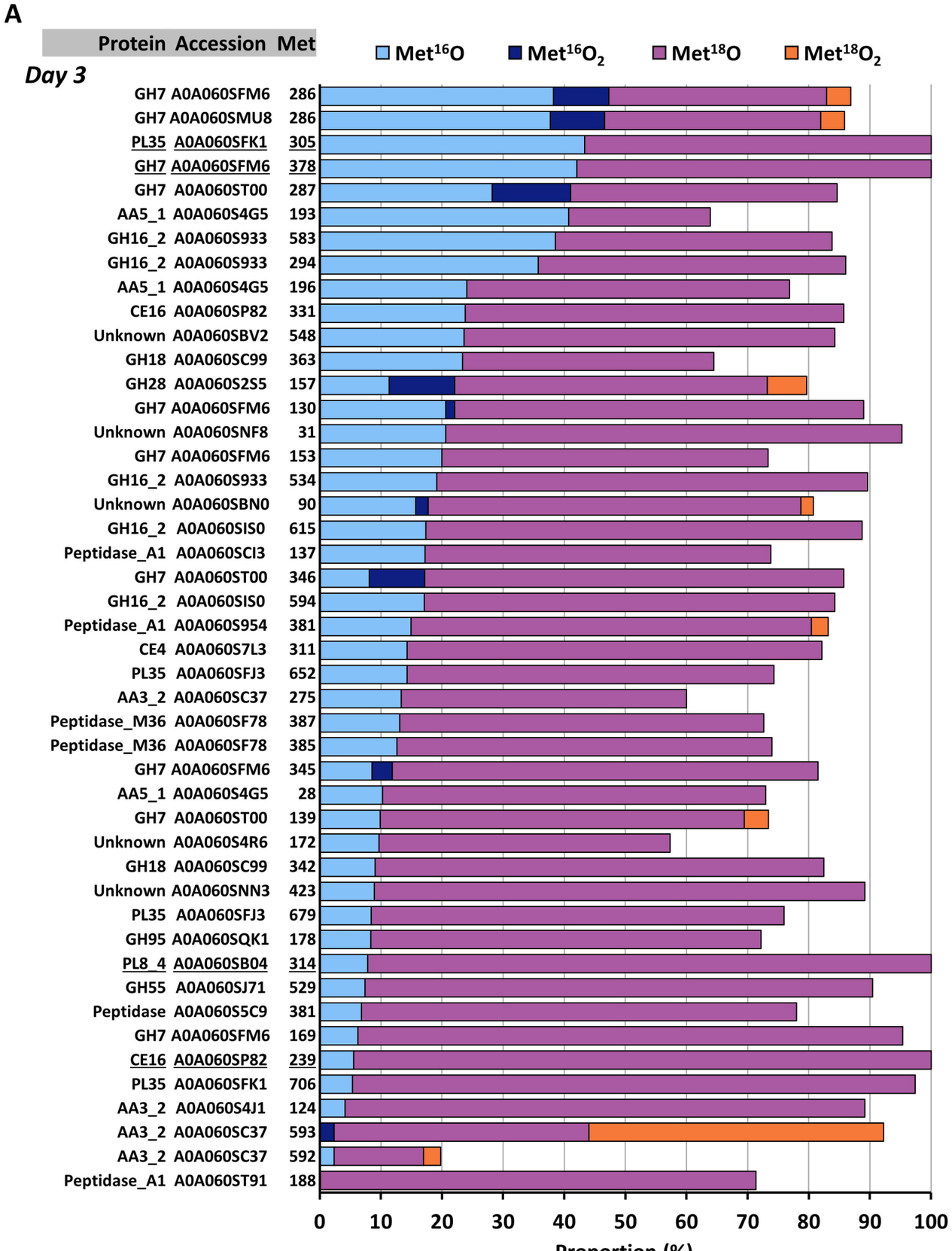
A
Protein Accession Met
Met16O
Met16O2
Met18O
Met18O2
Day 3
GH7 A0A060SFM6 286
GH7 A0A060SMU8 286
PL35 A0A060SFK1 305
GH7 A0A060SFM6 378
GH7 A0A060ST00 287
AA5_1 A0A060S4G5 193
GH16_2 A0A060S933 583
GH16_2 A0A060S933 294
AA5_1 A0A060S4G5 196
CE16 A0A060SP82 331
Unknown A0A060SBV2 548
GH18 A0A060SC99 363
GH28 A0A060S2S5 157
GH7 A0A060SFM6 130
Unknown A0A060SNF8 31
GH7 A0A060SFM6 153
GH16_2 A0A060S933 534
Unknown A0A060SBN0 90
GH16_2 A0A060SIS0 615
Peptidase_A1 A0A060SCI3 137
GH7 A0A060ST00 346
GH16_2 A0A060SIS0 594
Peptidase_A1 A0A060S954 381
CE4 A0A060S7L3 311
PL35 A0A060SFJ3 652
AA3_2 A0A060SC37 275
Peptidase_M36 A0A060SF78 387
Peptidase_M36 A0A060SF78 385
GH7 A0A060SFM6 345
AA5_1 A0A060S4G5 28
GH7 A0A060ST00 139
Unknown A0A060S4R6 172
GH18 A0A060SC99 342
Unknown A0A060SNN3 423
PL35 A0A060SFJ3 679
GH95 A0A060SQK1 178
PL8_4 A0A060SB04 314
GH55 A0A060SJ71 529
Peptidase A0A060S5C9 381
GH7 A0A060SFM6 169
CE16 A0A060SP82 239
PL35 A0A060SFK1 706
AA3_2 A0A060S4J1 124
AA3_2 A0A060SC37 593
AA3_2 A0A060SC37 592
Peptidase_A1 A0A060ST91 188
0 10 20 30 40 50 60 70 80 90 100
Proportion (%)

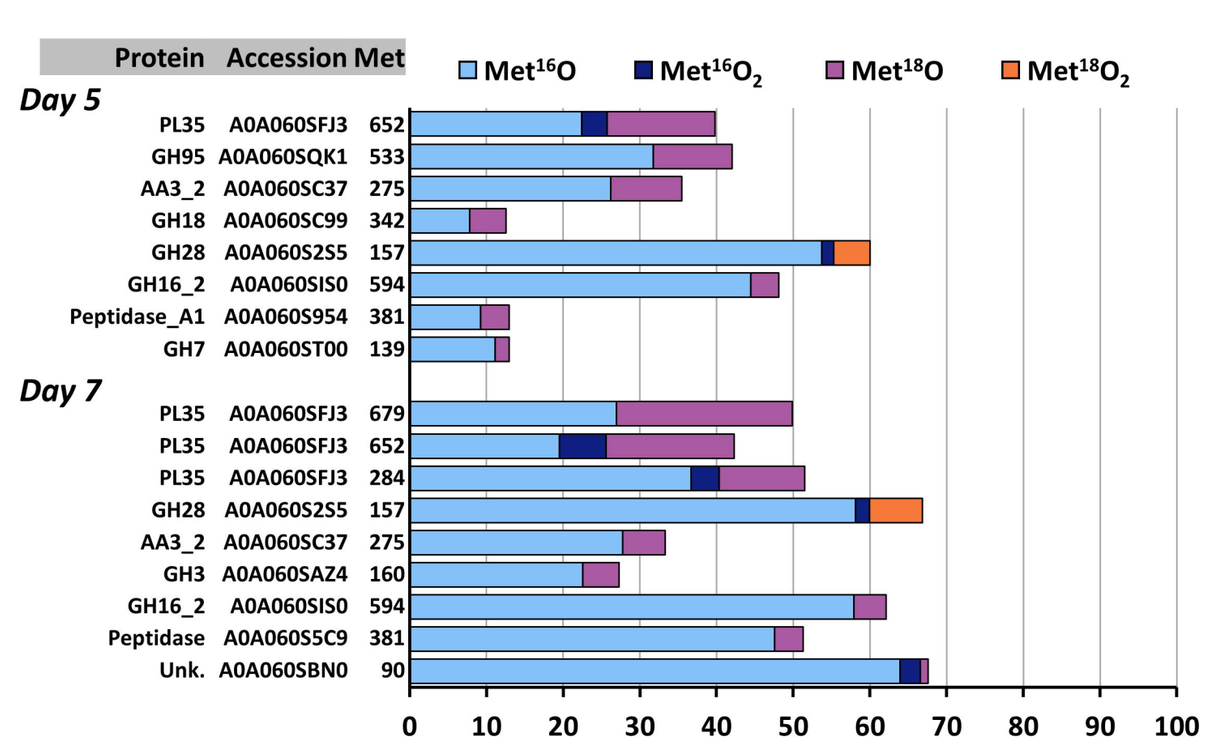
B
Protein Accession Met
Met16O
Met16O2
Met18O
Met18O2
Day 5
PL35 A0A060SFJ3 652
GH95 A0A060SQK1 533
AA3_2 A0A060SC37 275
GH18 A0A060SC99 342
GH28 A0A060S2S5 157
GH16_2 A0A060SIS0 594
Peptidase_A1 A0A060S954 381
GH7 A0A060ST00 139
Day 7
PL35 A0A060SFJ3 679
PL35 A0A060SFJ3 652
PL35 A0A060SFJ3 284
GH28 A0A060S2S5 157
AA3_2 A0A060SC37 275
GH3 A0A060SAZ4 160
GH16_2 A0A060SIS0 594
Peptidase A0A060S5C9 381
Unk. A0A060SBN0 90
0 10 20 30 40 50 60 70 80 90 100

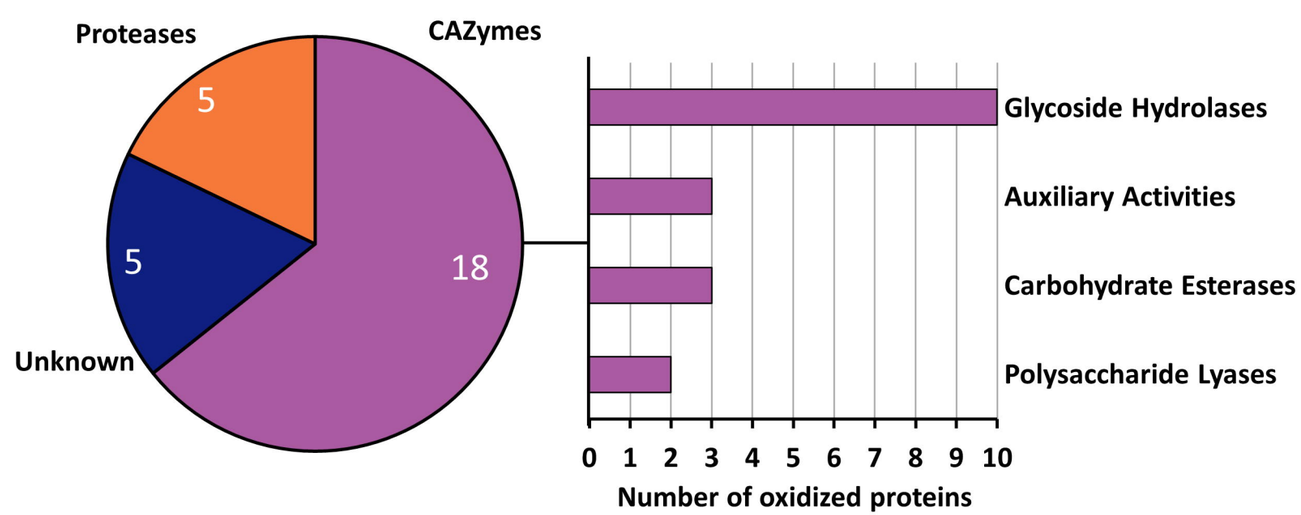
C
Proteases
CAZymes
Unknown
5
5
18
Glycoside Hydrolases
Auxiliary Activities
Carbohydrate Esterases
Polysaccharide Lyases
0 1 2 3 4 5 6 7 8 9 10
Number of oxidized proteins

A

```
                                  130                 139                                 153                                                 169
A  A0A060SFM6  127  V Y L M D S S D Q K Y Q I F N L K N Q E F T F D V D M S K L P C G L N G A L Y F V E M D A D G G V S  176
B  A0A060ST00  127  V Y L L S E D D T T Y E M F N L K N Q E F T F D V D M S T L P C G L N G A L Y F V E M D A D G G K S  176
C  A0A060SMU8  127  V Y L M G T D D A S Y Q L F N L K N Q E F T F D V D M S N L P C G L N G A L Y F V E M D A D G G K S  176

                                 286/287                                                                  343/344   345/346
A  A0A060SFM6  281  F N S W R M G D Q T F L G P G K T V N  299  338  A N S K T N I P G M A T Y D S I T D S F C N A Q  359
B  A0A060ST00  282  F N S W R M G D Q T F L G S G K T V D  300  339  A N S K T N I P G M A A Y D S I T D D F C N A Q  360
C  A0A060SMU8  281  F N S F R M G N Q T F L G P G K I V N  299  338  A N S K T N I P G L A T F D S I T D E F C N A Q  359

                                                 378                                                  422   424         430/431
A  A0A060SFM6  366  T N S F E K L G G L K Q M G A S F D K G  385  420  R G P C P T T S G Q P T D V E S Q S P D A T  441
B  A0A060ST00  367  T N T F E S L G G L K Q M G N A F Q Q G  386  421  R G P C P T S S G Q P T D V E S Q S P G A T  442
C  A0A060SMU8  366  T N T F E Q L G G L Q Q M G N S F Q K G  385  420  R G P C P A N S G I P A T I E Q T E A S A S  441
```

B

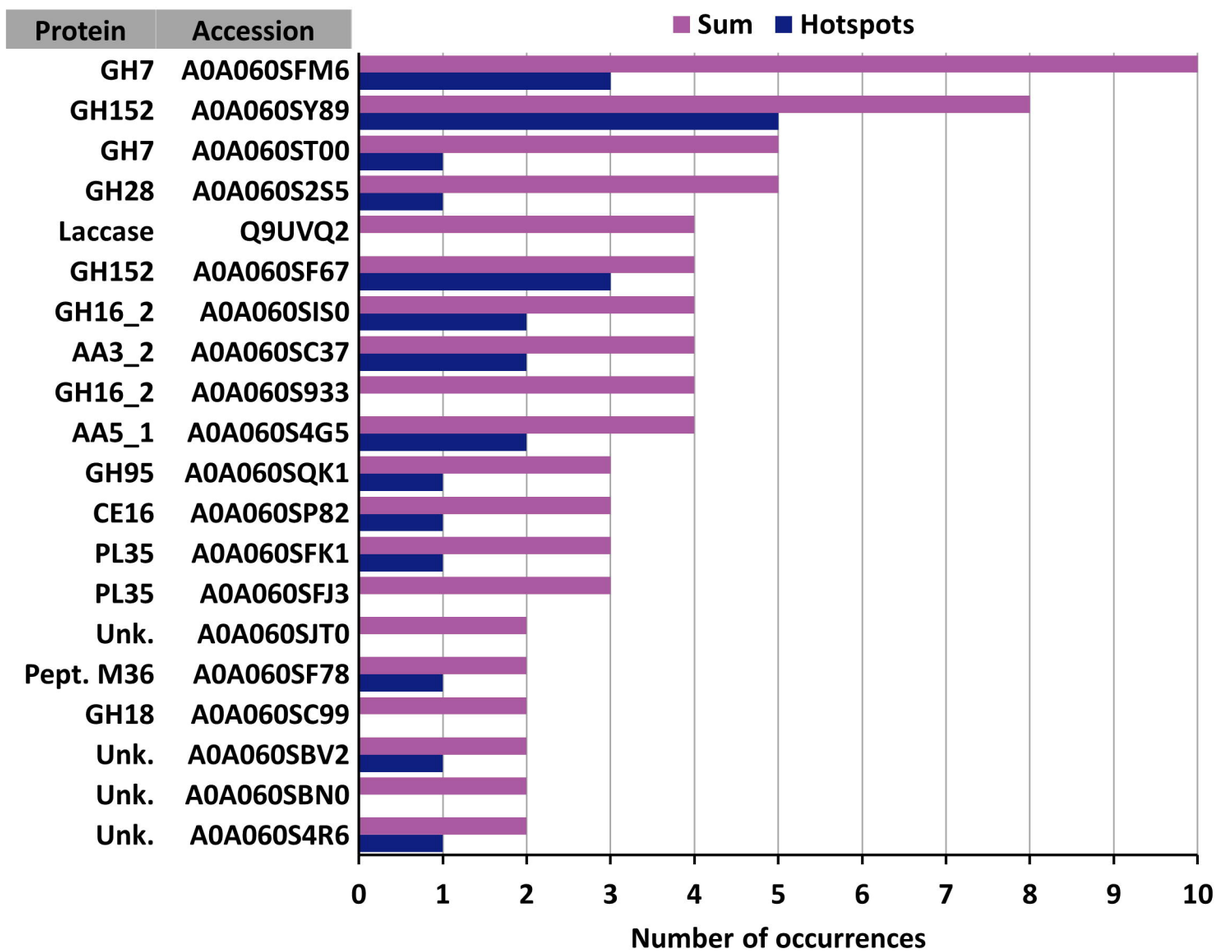
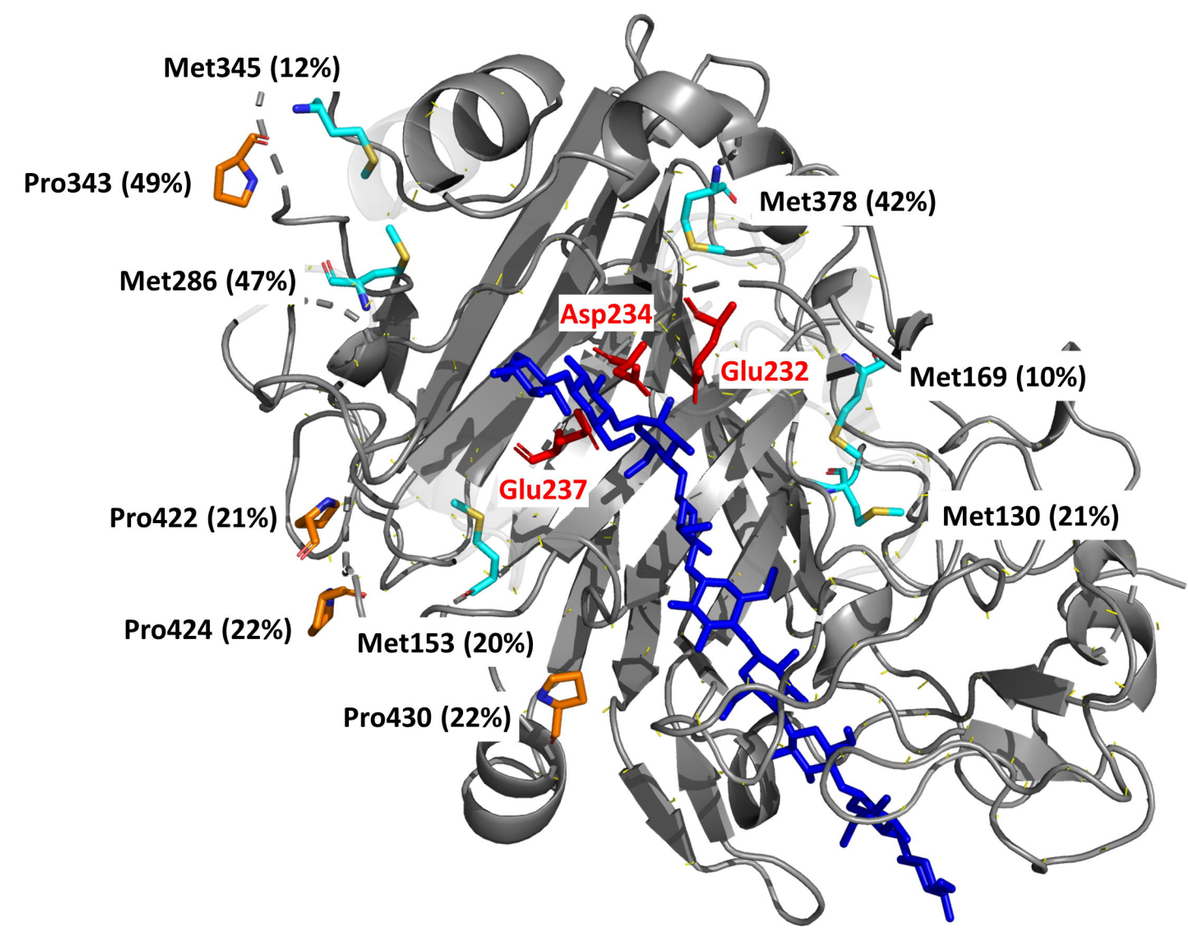
C